JCI The Journal of Clinical Investigation

# Kidney-specific WNK1 amplifies kidney tubule responsiveness to potassium via WNK body condensates

Cary R. Boyd-Shiwarski, … , Ossama B. Kashlan, Arohan R. Subramanya

*J Clin Invest.* 2025. https://doi.org/10.1172/JCI188792.

Research In-Press Preview Cell biology Nephrology

## Graphical abstract

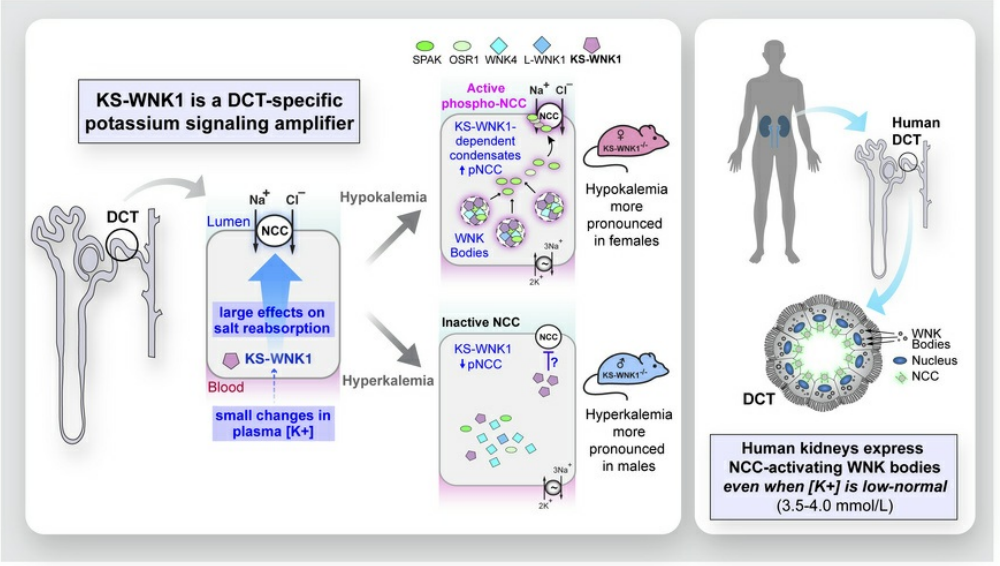


## Find the latest version:

https://jci.me/188792/pdf

# Kidney-specific WNK1 amplifies kidney tubule responsiveness to potassium via WNK body condensates

Cary R. Boyd-Shiwarski[1,2,*], Rebecca T. Beacham[1], Jared A. Lashway[1], Katherine E. Querry[1], Shawn E. Griffiths[1], Daniel J. Shiwarski[3,4], Sophia A. Knoell[1], Nga H. Nguyen[1], Lubika J. Nkashama[1], Melissa N. Valladares[1], Anagha Bandaru[1], Allison L. Marciszyn[1], Jonathan Franks[5], Mara Sullivan[5], Simon C. Watkins[2,5,6], Aylin R. Rodan[7,8,9,10], Chou-Long Huang[11], Sean D. Stocker[12], Ossama B. Kashlan[1,2,13], Arohan R. Subramanya[1,2,6,14]

[1]Department of Medicine, Renal-Electrolyte Division, University of Pittsburgh, Pittsburgh, PA, USA
[2]Pittsburgh Center for Kidney Research, University of Pittsburgh School of Medicine, Pittsburgh, PA, USA
[3]Department of Medicine, Vascular Medicine Institute, University of Pittsburgh, PA, USA
[4]Department of Bioengineering, Swanson School of Engineering, University of Pittsburgh, Pittsburgh PA, USA
[5]Center for Biological Imaging, University of Pittsburgh, Pittsburgh, PA, USA
[6]Department of Cell Biology, University of Pittsburgh, Pittsburgh, PA, USA
[7]Department of Internal Medicine, Division of Nephrology and Hypertension, University of Utah, Salt Lake City, UT, USA
[8]Department of Human Genetics, University of Utah, Salt Lake City, UT, USA
[9]Molecular Medicine Program, University of Utah, Salt Lake City, UT, USA
[10]Medical Service, VA Salt Lake City Healthcare System, Salt Lake City, UT, USA
[11]Department of Internal Medicine, Division of Nephrology and Hypertension, University of Iowa Carver College of Medicine, Iowa City, Iowa, USA
[12]Department of Neurobiology, University of Pittsburgh, Pittsburgh, PA, USA
[13]Department of Computational and Systems Biology, University of Pittsburgh, Pittsburgh, PA, USA
[14]VA Pittsburgh Healthcare System, Pittsburgh, PA, USA

[*]Corresponding Author:
Cary R. Boyd-Shiwarski
S933 Scaife Hall
3550 Terrace St
Pittsburgh, PA 15261
(412) 624-3669
boydcr@upmc.edu

Conflict of Interest Statement: The authors have declared that no conflict of interest exists

**Abstract**

To maintain potassium homeostasis, the kidney's distal convoluted tubule (DCT) evolved to convert small changes in blood [$K^+$] into robust effects on salt reabsorption. This process requires NaCl cotransporter (NCC) activation by the With-No-Lysine (WNK) kinases. During hypokalemia, the Kidney-Specific WNK1 isoform (KS-WNK1) scaffolds the DCT-expressed WNK signaling pathway within biomolecular condensates of unknown function termed WNK bodies. Here, we show that KS-WNK1 amplifies kidney tubule reactivity to blood [$K^+$], in part via WNK bodies. Genetically modified mice with targeted condensate disruption trap the WNK pathway, causing renal salt wasting that is more pronounced in females. In humans, WNK bodies accumulate as plasma potassium falls below 4.0 mmol/L, suggesting that the human DCT experiences the stress of potassium deficiency even when [$K^+$] is in the low-normal range. These data identify WNK bodies as kinase signal amplifiers that mediate tubular [$K^+$] responsiveness, nephron sexual dimorphism, and blood pressure salt-sensitivity. Our results illustrate how biomolecular condensate specialization can optimize a mammalian physiologic stress response that impacts human health.

**Keywords**

WNK Lysine-Deficient kinase 1, distal kidney tubules, thiazide-sensitive Na-Cl cotransporter, Solute Carrier Family 12 Member 3, biomolecular condensates, sexual dimorphism, salt-sensitive hypertension, potassium homeostasis.

## Introduction

During environmental stress, physiologic systems must sense imbalance and coordinate appropriately tuned responses that maintain homeostasis. An example of this is the distal nephron, a series of kidney tubule segments which sense and cooperatively maintain plasma potassium concentrations within the narrow physiologic window required for life (1). During the stress of hypokalemia, a serine-threonine kinase cascade within the distal convoluted tubule (DCT) activates the thiazide-sensitive NaCl cotransporter (NCC; *SLC12A3*) via phosphorylation (2). Hypokalemia-mediated NCC activation limits downstream delivery of sodium to the connecting tubule and collecting duct, diminishing distal voltage-dependent potassium secretion. This minimizes urinary cation losses to conserve total body potassium (3). In contrast, hyperkalemia inhibits NCC, facilitating kaliuresis (4).

With-No-Lysine (WNK) kinases are essential regulators of NCC phosphorylation and potassium homeostasis. During hypokalemia, the WNKs activate the kinases SPAK (*STK39*) and OSR1 (*OXSR1*), which phosphorylate NCC directly(1). Conversely, hyperkalemia promotes NCC dephosphorylation (4, 5). The integration of these signals generates an inverse relationship between NCC phosphorylation status and plasma [$K^+$] (6). The importance of WNK signaling in potassium metabolism is evidenced by Familial Hyperkalemic Hypertension (FHHt), a Mendelian syndrome caused by overactivation of the DCT-expressed WNK signaling pathway, resulting in NCC hyperphosphorylation, salt-sensitive hypertension, and hyperkalemia that is cured with thiazide diuretics (7, 8).

The distal convoluted tubule (DCT) features a unique complement of WNK-SPAK/OSR1 pathway gene products. WNK4 is the dominant DCT-expressed WNK kinase (9). The full-length kinase-active "Long" isoform of WNK1 (L-WNK1) is also expressed in this nephron segment, though its abundance is low (10). Instead, the most abundant WNK1 isoform in the DCT is a kidney-exclusive truncated gene product that lacks kinase activity. This "Kidney-Specific WNK1" (KS-WNK1) isoform requires an intragenic promoter located within intron 4 of the *WNK1* gene (Figure 1A). This distal tubule-specific promoter drives the expression of an alternative first exon that replaces the L-WNK1 N-terminus and most of the kinase domain with 30 unique amino acids encoded by exon 4a (11). Downstream from this sequence, L-WNK1 and KS-WNK1 are identical (Figure 1B). Exon 4a emerged during the evolutionary transition of vertebrates from water to land, a process that required robust kidney tubular transport to preserve electrolyte homeostasis (12, 13). Exon 4a is also critical for the formation of WNK signaling puncta during hypokalemia. These KS-WNK1 dependent foci, termed WNK bodies, influence the spatial localization of the DCT WNK-SPAK/OSR1 pathway (12) (Figure 1C). Hypokalemic WNK bodies contain WNK4, L-WNK1, SPAK, and OSR1, and their appearance correlates with NCC activation (12, 14, 15), suggesting that KS-WNK1's role in WNK body formation is linked to sodium transport.

WNK bodies are micron-sized spheroid non-membrane bound low-density regions of the cytoplasm that fail to colocalize with conventional organelle markers (12, 14, 16) (Figure 1). Thus, they are biomolecular condensates—membraneless cytosolic foci that assemble via phase transitions (17, 18).Though KS-WNK1 dependent WNK bodies are exclusive to the distal nephron, WNK kinases such as L-WNK1 and WNK3 are more ubiquitously expressed, and their ability to form condensates is a fundamental property that allows them to control ion transport and cell

volume in many cell types (17, 19). For example, during acute hypertonic cell shrinkage, L-WNK1, SPAK, and OSR1 undergo crowding-induced phase separation, causing their rapid activation within cytosolic liquid-like droplets. Following activation, SPAK and OSR1 leave these dynamic structures and accumulate at the plasma membrane to phosphorylate NKCC1 (*SLC12A2*) and KCCs (*SLC12A4-7*), ubiquitously expressed NCC-like cotransporters that coordinate cell volume recovery. L-WNK1-dependent phase separation is mediated by its large C-terminal domain (CTD), a >100kDa intrinsically disordered region (IDR) that efficiently condenses in response to crowding (17) (Figure 1B). Notably, the truncated KS-WNK1 isoform lacks intrinsic kinase activity but contains the entire disordered C-terminal domain; in fact, this large phase separation-driving IDR comprises greater than 90% of the entire KS-WNK1 protein (Figure 1, B and D). This strongly suggests that KS-WNK1 functions as an intrinsically disordered scaffold that coordinates WNK4-SPAK/OSR1 activity in the DCT via condensed phase signaling (20).

Though KS-WNK1 mediates distal tubule WNK body assembly, its physiologic role in NCC regulation remains unresolved. Here, we report that KS-WNK1 functions as an amplifier of the WNK signaling pathway that operates across the entire physiologic range of $[K^+]$, allowing the DCT to optimize NCC-mediated salt reabsorption in response to potassium imbalance. By employing mouse models of KS-WNK1 absence and dysfunction, we demonstrate that this effect is WNK body-dependent, establishing a previously unrecognized role for biomolecular condensates in mammalian potassium and blood pressure homeostasis. We further show that the effect is sex-specific, as females require WNK body-mediated signaling to amplify DCT salt reabsorption during hypokalemia. Finally, we show that in the human kidney, WNK body expression progressively increases at a $[K^+]$ below 4.0 mmol/L, suggesting condensate-mediated

activation of tubular salt reabsorption when potassium concentrations are within the low-normal reference range. This suggests a role for WNK bodies in human salt-sensitive hypertension. Together, our results identify WNK bodies as kidney-specific signaling condensates that regulate blood pressure and potassium homeostasis.

**Results:**

***KS-WNK1 amplifies the inverse relationship between NCC phosphorylation and blood [$K^+$] via multiple mechanisms.***

To begin to understand the role of KS-WNK1-dependent WNK bodies in NCC regulation, we studied the effect of KS-WNK1 deletion on NCC expression and phosphorylation status in mice across a broad range of blood potassium concentrations. KS-WNK1 KO mice and wild-type littermates (WT) were administered diets with low $K^+$ (LK), control, or alkaline high $K^+$ ("high $K^+$ basic"; HKB) content for 10 days (Table S1). Because $K^+$ loaded mice with a normal glomerular filtration rate efficiently excrete a potassium load (1, 21), we also studied a cohort of HKB-fed mice supplemented with the potassium-sparing diuretic amiloride (2mg/kg/day) to induce frank hyperkalemia (Table S2). We then performed immunoblots for total NCC (tNCC) and phospho-Thr53 NCC (pNCC), a signature of NCC activation (Figure 2, A-C, S2, A-H, S3, A-D).

We initially compared NCC densitometry in WT and KS-WNK1 KO mice stratified by sex and dietary $K^+$ maneuver. While this analysis did not reveal a significant effect of KS-WNK1 deletion on tNCC protein abundance (Figure 2, D and E), KS-WNK1 KO mice exhibited lower pNCC abundance during $K^+$ restriction and higher pNCC abundance during $K^+$ loading with amiloride (Figure 2, F and G). The effects of HKB plus amiloride on pNCC were confirmed with antibodies

that recognize alternative NCC phosphoactivation sites at threonine-58 and serine-71 (Figure S3B) (22). KS-WNK1 KO mice also exhibited higher pNCC abundance than WT controls following 10d of potassium loading on a high KCl (5% potassium) diet (Figure S4, A-C), which was sufficient to induce frank hyperkalemia in the absence of amiloride (Figure S4, D and E). Thus, the effects of KS-WNK1 on pNCC during hyperkalemia were consistent across different physiologic maneuvers. The requirement of KS-WNK1 expression for $K^+$ induced inhibition of pNCC is supported by prior publications (23, 24). Collectively, these data indicate that KS-WNK1 exerts divergent effects on pNCC depending on blood potassium status. During hypokalemia, KS-WNK1 appears to be an *activator* of NCC, but during hyperkalemia, it appears to be an NCC *inhibitor* (Figure 2H). These findings comport with a recent report (23) and suggest that KS-WNK1 exerts complex effects on NCC activity that span the full physiologic spectrum of blood $[K^+]$.

To further explore these findings, we performed a regression analysis, plotting individual tNCC and pNCC densitometry values for mice subjected to the low $K^+$, control, HKB, and HKB plus amiloride maneuvers, as a function of blood potassium concentration measured at the time of sacrifice (Figure 3, A-C). For WT mice, these graphs revealed a steep increase in pNCC abundance below a potassium concentration of 4mmol/L, indicating a nonlinear relationship between NCC phosphorylation and blood $[K^+]$. This amplification effect was evident in the pNCC and pNCC/tNCC graphs and was clearly blunted in KS-WNK1 KO mice (Figure 3, B and C). We first attempted to fit these data to single exponential curves, but this model was inadequate, as it overestimated nearly all the measured NCC densitometry values at a blood $[K^+] > 6$mmol/L for WT mice (Figure 3, A-C; compare WT filled blue circles that consistently fall below the curve).

Thus, to stabilize variance in NCC signal across measured blood [$K^+$] and better visualize goodness-of-fit, we log-transformed the densitometry data (Figure 3, D-F). As predicted by the suboptimal single exponential fits to the untransformed data, simple linear regression of these log-transformations resulted in non-random residuals for WT mice, strongly suggesting that additional components are required to adequately model the observed NCC densitometry dependence on blood [$K^+$](Figure S5A).

Subsequent curve-fitting trials revealed that the WT log-transformed data were best explained by a *segmental linear regression* model, which added 2 parameters: a second slope and a breakpoint dividing the segments ($X_0$; Figure 3, D-F). For WT mice, the addition of a second linear component yielded symmetric and randomly distributed residuals, significantly improving the fit ($p \leq 0.0001$ vs straight line by F-test for all three WT curves (tNCC, pNCC, and pNCC/tNCC), (Figure S5A). Remarkably, the tNCC, pNCC, and pNCC/tNCC breakpoints consistently settled at a blood [$K^+$] around 5.6 mmol/L; i.e., near the upper limit of the currently defined normal reference range for serum (25). In contrast to WT mice, the tNCC, pNCC, and pNCC/tNCC data in KS-WNK1 KO mice were best-fit by simple linear regression (Figure 3, D-F), as goodness-of-fit was not improved by segmental linear regression. Furthermore, simple linear regression yielded symmetric and randomly distributed residuals for the KO data (Figure S5B). These results indicate that while both WT and KS-WNK1 KO mice exhibit an inverse relationship between NCC and blood [$K^+$], the WT mice require an additional component to account for the relationship between NCC and blood [$K^+$] during hyperkalemia. These findings were concordant in males and females when the pNCC data were disaggregated by sex (Figure S5, C-F).

This regression analysis uncovered key differences in the relationship between blood potassium and pNCC in WT and KS-WNK1 KO mice. At a [$K^+$] less than 5.6 mmol/L (i.e., $X<X_0$), the log-transformed WT and KO slopes of pNCC and pNCC/tNCC were not different, but the Y-intercepts for pNCC and pNCC/tNCC were significantly lower in KS-WNK1 KO mice ($p= 0.0002$ and 0.0102 for pNCC and pNCC/tNCC respectively; Figure 3, E and F). Thus, when blood potassium is <5.6 mmol/L, NCC phosphorylation status increases exponentially in both WT and KS-WNK1 KO mice as plasma $K^+$ gets progressively lower, an amplification effect that is significantly blunted in mice lacking KS-WNK1. At a blood potassium greater than 5.6mmol/L ($X>X_0$), the inverse relationship between [$K^+$] and pNCC increased dramatically in WT mice, resulting in a marked negative deflection in slope (Figure 3, E and F, S5, D and F). This suggests that WT mice recruit an auxiliary process that further suppresses NCC phosphorylation when blood [$K^+$] >5.6 mmol/L. Because this deflection in slope is absent in KO mice, the auxiliary dephosphorylation mechanism appears to be KS-WNK1-dependent.

Collectively, these data suggest that KS-WNK1 steepens the inverse relationship between blood [$K^+$] and NCC activation through discrete mechanisms that differentially affect NCC phosphorylation and dephosphorylation. In other words, KS-WNK1 *expands the dynamic range* of NCC phosphorylation status in response to changes in blood [$K^+$], converting small changes in plasma potassium into large effects on pNCC abundance.

***Relationship between blood [$K^+$] and WNK body expression***.

We hypothesized that the potassium-dependent changes in NCC phosphorylation status correspond with altered WNK body expression. To test this, we performed DCT immunostaining

for WNK bodies in kidneys harvested from WT male mice with a broad range of blood potassium concentrations. As blood potassium levels progressively decreased below 4 mmol/L, WNK body size increased exponentially (Figure 4, A and B). By contrast, WNK bodies were not visible in WT males with a plasma potassium greater than 4.0 mmol/L. Thus, similar to the effects of hypokalemia on pNCC abundance, WNK body expression correlates inversely with changes in blood [$K^+$] (Figure 4C). This suggests that the nucleation and growth of these condensates is linked to the amplification of NCC activity during potassium deficiency.

We have previously published that in an in vitro cellular model exogenous WNK bodies have distinct ultrastructures that are electron hypodense, membraneless assemblies that do not colocalize with conventional organelle markers (12). Using a correlative light and electron microscopy (CLEM) method that combines confocal microscopy with backscattered electron detection via scanning electron microscopy (BSD-SEM) on semithin kidney sections revealed that endogenous WNK bodies have similar properties (Figure 4D).

***KS-WNK1 increases WNK-SPAK/OSR1 pathway abundance during $K^+$ deficiency but does not influence its abundance during $K^+$ excess.*** The DCT-expressed WNK4-SPAK/OSR1 pathway constitutes the canonical NCC activation signal (8). Given the role of WNK bodies in controlling its localization, we interrogated this signaling cascade in KS-WNK1 KO mice. Consistent with prior reports (2, 26), $K^+$ restriction in WT mice upregulated the expression of WNK4, total (t)SPAK, and phospho-(p) Ser 373 SPAK/p Ser 325 OSR1 relative to control diets (Figure 5, A and D). By comparison, $K^+$ restricted KS-WNK1 KO mice exhibited weaker WNK4-SPAK/OSR1 pathway upregulation (Figure 5, A and D). We did not observe a difference in pSPAK normalized

to tSPAK in WT and KO on low $K^+$, contrary to prior reports (23)(Figure 5E). In contrast to the low $K^+$ maneuver, WT and KO mice exhibited no differences in WNK4, tSPAK, or pSPAK/pOSR1 expression in the context of HKB or HKB plus amiloride treatments that increase blood [$K^+$] (Figure 5, B, C, F). This supports findings by Penton *et al.* who demonstrated that high $K^+$ directly and rapidly controls NCC phosphorylation independent of the SPAK/OSR1 pathway (27). Thus, the ability of KS-WNK1 to amplify NCC phosphorylation during $K^+$ deficiency correlates with increased WNK4-SPAK/OSR1 signaling via WNK bodies, but its ability to augment NCC dephosphorylation during $K^+$ excess does not (Figure 5G).

***KS-WNK1 and WNK body localization.*** Because the effect of KS-WNK1 on WNK-SPAK/OSR1 signaling likely predominates when hypokalemia-induced WNK bodies are present (12), we evaluated the effects of KS-WNK1 deletion on WNK-SPAK/OSR1 localization during dietary $K^+$ restriction. Consistent with our prior report (12), $K^+$ restriction was associated with the formation of DCT-specific WNK bodies that stained positive for WNK1, WNK4, and pSPAK/pOSR1, suggesting that WNK4 activates its downstream targets within condensates (Figure 6A). These structures were largely absent in potassium-deficient KS-WNK1 KO mice regardless of sex (Figure 6, A and D). Even so, pSPAK/pOSR1 apical staining was present despite KS-WNK1 deletion (Figure 6B), indicating that KS-WNK1 is not necessary for active SPAK to engage with NCC during hypokalemia. However, given the observation that KS-WNK1 KO mice exhibit blunted SPAK/OSR1 and NCC phosphorylation during $K^+$ deficiency (Figure 2, A and G, 3, B and E, 5, A and D), the data indicate that KS-WNK1 potentiates SPAK/OSR1 activation in response to decreased blood [$K^+$], likely through WNK body-mediated signaling.

As reported previously (12), KS-WNK1 KO DCT cells rarely exhibited WNK-SPAK/OSR1 positive puncta that were mislocalized to the basal pole during $K^+$ restriction (Figure 6B, arrowheads). Morphometric analysis (Figure 6C) revealed that while both sexes exhibited a comparable number of WNK bodies per cell during $K^+$ restriction (Figure 6D), females exhibited larger condensates that were positioned closer to the tubular lumen (Figure 6, E and F). These findings suggest sex-specific differences in WNK-SPAK/OSR1 pathway functionality.

***Sex-specific effects of KS-WNK1 on blood and urine electrolytes.*** We also observed diverging trends between WT and KS-WNK1 KO mice when blood and urine data were disaggregated by sex. Sex-dependent differences were more evident at the extremes of low and high $K^+$ and included effects on blood $K^+$, $Cl^-$, $HCO_3^-$, $Ca^{2+}$, and urine osmolarity and pH. When placed on a $K^+$ deficient diet, where NCC phosphorylation is high and KS-WNK1 dependent (Figure 2), KS-WNK1 KO females exhibited more pronounced hypernatremia, hypokalemia, and reduced urine osmolality compared to WT females (Figure 7, A-C, Table S2 and S3). We did not observe differences in urine $K^+$ as these measurements were at the low limit of detection on a $K^+$ deficient diet (Table S3). In contrast to females, KS-WNK1 KO males did not exhibit lower blood $K^+$ versus WT males during potassium restriction (Figure 7C), despite strong effects of KS-WNK1 deletion on pNCC abundance (Figure 2). Male KS-WNK1 KO mice also did not exhibit differences in blood $Na^+$ or urine osmolality. Relative to WT littermates, however, male KS-WNK1 KO mice were more hypercalcemic during $K^+$ restriction (Figure 7D, Table S2). Thus, $K^+$-restricted KS-WNK1 KO mice exhibit features commonly seen in states of low NCC activity—low blood potassium levels and higher blood calcium levels—similar to Gitelman syndrome or thiazide diuretic administration (8).

Next, we investigated whether the relative hypokalemia in $K^+$ restricted KS-WNK1 KO females was due to increases in aldosterone, ENaC, or ROMK—known factors that can cause hypokalemia. During dietary $K^+$ restriction, aldosterone (aldo) levels tended to be equal to or lower in KS-WNK1 KO mice (Table S2), consistent with prior observations (28). While it is conceivable that lower aldo levels observed in KS-WNK1 KO mice could be explained by increased ENaC activation, we observed the opposite, with lower expression of the uncleaved form of γENaC (Figure S7, A-C) and could not detect expression of the subunit's cleaved/active form in either WT or KO mice during dietary $K^+$ restriction (Figure S7, A-C). Collectively, these findings suggest that the hypokalemia in female KS-WNK1 KO mice is not due to increased aldo or ENaC, but instead reduced NCC activity. Others have reported that KS-WNK1 KO mice have decreased ENaC expression (28, 29), possibly to compensate for increased NCC activity. We also found that ROMK protein abundance was not elevated in KS-WNK1 KO female mice relative to WT sex-matched littermates (Figure S7, D and E). While we did not observe KS-WNK1 induced changes to ROMK abundance, earlier in vitro studies suggest that KS-WNK1 promotes ROMK activation (30, 31). Mouse models have shown that KS-WNK1 KO mice exhibit reduced ROMK activity (24, 32), despite an increased localization of ROMK at the apical membrane in KS-WNK1 KO mice (28, 29). Further research is needed to understand how KS-WNK1 and ROMK interact and regulate serum potassium levels across the range of blood $K^+$.

***Role of KS-WNK1 in blood pressure regulation, salt sensitivity, and thiazide responsiveness***. Given the importance of NCC in blood pressure regulation (3), we performed telemetric blood pressure measurements in KS-WNK1 KO mice (Figure 8A). These studies focused on females

since they exhibited larger electrolyte differences during $K^+$ restriction (Figure 7). Despite differences in pNCC expression (Figure 2), ten days of potassium deprivation yielded no differences in mean arterial pressure (MAP) between WT and KS-WNK1 KO females (Figure 8B). Moreover, though $K^+$ restricted WT and KO mice both developed a salt-sensitive increase in blood pressure (21), we observed no differences between knockout mice and WT littermates. Female mice administered a control diet for 10 days did not exhibit changes in blood pressure, either at baseline or after saline-loading, regardless of KS-WNK1 genotype (Figure 8B). To test for differences in NCC activity, we challenged WT and KS-WNK1 KO mice with an intraperitoneal injection of hydrochlorothiazide (HCTZ; 25mg/kg). WT mice on $K^+$ restriction responded to HCTZ injection with a significant 4.5 mmHg average decrease in MAP. In contrast, KS-WNK1 KO mice were relatively insensitive to HCTZ (Figure 8C). Thus, similar to humans with Gitelman syndrome (33), $K^+$ restricted KS-WNK1 KO female mice exhibit low NCC activity but are able to maintain their blood pressure via compensatory effects.

To further assess the effects of KS-WNK1 on NCC activation, we administered HCTZ and measured urinary volume, $Na^+$, $K^+$, and $Cl^-$ in male and female mice maintained on either a low $K^+$ or control diet for 10 days (Figure 8D). $K^+$ restricted KS-WNK1 KO mice exhibited a blunted response to HCTZ compared to WT littermates, with decreased urinary volume and $UNa^+V$ (Figure 8, E and F). There was no change in urinary $K^+$, likely because it was near the lower limit of detection due to dietary $K^+$ restriction (Figure 8G). There was also a trend for decreased urinary $Cl^-$ under potassium restricted conditions (Figure 8H). These diuretic and natriuretic responses reflect lower NCC activity in KS-WNK1 KO mice compared to WT controls, consistent with the reduced NCC phosphorylation in KS-WNK1 KO mice after dietary $K^+$ restriction (Figure 2 & 3).

Interestingly, a previous study reported conflicting results, showing that KS-WNK1 KO mice exhibited increased thiazide-sensitivity on a control diet (24). These discrepancies could be due to differences in composition of the control diet or that the WT control mice in the prior study were not littermate controls.

***WNK bodies are required for NCC activation during hypokalemia***.

Our analyses in knockout mice demonstrate that during potassium deficiency, KS-WNK1 drives WNK body formation (Figure 6), amplifies NCC phosphoactivation (Figure 3), and increases WNK4-SPAK/OSR1 pathway expression (Figure 5). However, these studies do not establish whether the blunted NCC activation in $K^+$ restricted KS-WNK1 KO mice is specifically due to impaired WNK body condensation or other KS-WNK1 dependent factors. To address this, we generated a mouse expressing a full-length mutant version of KS-WNK1 that cannot form functional WNK bodies. As noted in Figure 1, the KS-WNK1 N-terminus is capped by 30 unique amino acids encoded by exon 4a. Previously, we showed that the exon 4a coding sequence contains a conserved cysteine-rich hydrophobic (CRH) motif that is necessary for WNK body formation in vitro (12). To disrupt WNK body formation in mice, we replaced five essential hydrophobic residues within the CRH motif with five neutral glutamines (VFVIV->QQQQQ) (Figure 9A, S8, A-D). AlphaFold predicts this "5Q" mutation disrupts KS-WNK1 N-terminal structure, unraveling an amphipathic helix encoded by exon 4a (Figure 9B).

Mice homozygous for the KS-WNK1 5Q mutation were maintained on control or low $K^+$ diet for 10 days and assessed for changes in SPAK/OSR1 and NCC activation by immunostaining, western blot, and electrolyte measurements. Potassium-restricted 5Q mice were unable to form spheroid

WNK bodies and instead formed larger amorphous aggregates with reduced roundness that accumulated around nuclei (Figure 9, C and D). These structures were enriched in pSPAK/pOSR1, which was absent from the apical membrane suggesting aberrant function (Figure 9E and F). Consistent with intracellular sequestration and disruption of signaling, during $K^+$ restriction pSPAK/pOSR1 abundance was increased in kidney immunoblots by 210% in males ($p = 0.0019$) and 136% in females ($p = 0.0032$), but pNCC abundance did not increase accordingly. Instead, pNCC decreased by 25% in males ($p = 0.018$) and 63% in females ($p = 0.0008$) (Figure 10, A-E).

Similar to KS-WNK1 KO mice, the effects of potassium restriction were predominantly observed in females. Potassium-restricted female 5Q mice had a significantly decreased blood $K^+$ and $Cl^-$, and increased $HCO_3^-$, suggestive of a sex-specific Gitelman-like phenotype (Table S4). Whereas 5Q mice fed a control diet had an opposing effect with males having the predominant phenotype exhibiting hyperchloremic metabolic acidosis (females trended toward this), with elevated $Cl^-$ and lower $HCO_3^-$. Collectively these findings indicate that the KS-WNK1 5Q mutation alters WNK body formation and function during $K^+$ restriction, resulting in mislocalization of the WNK-SPAK/OSR1 pathway and low NCC activity.

***WNK body abundance correlates with serum [$K^+$] in humans***. In WT mouse models, WNK bodies form during hypokalemia and disperse during normokalemia (12, 14) (Figure 4A). To date, human WNK bodies have only been reported in the setting of severe hypokalemic nephropathy, a pathologic condition caused by substantial $K^+$ deficiency (16). To explore the physiological relevance of WNK bodies in human health, we asked whether these potassium-dependent condensates are present in humans with [$K^+$] in the physiologic range (3.5-4.2 mmol/L). WNK

bodies were present in all 6 kidney samples studied from both male and female subjects ages 46-79 years (Figure 11A). Consistent with studies in mice, there was an inverse correlation between decreasing serum [$K^+$] and increasing WNK body abundance (Figure 11, B and C). A progressive increase in WNK bodies was noted, particularly when the measured [$K^+$] was <4.0mmol/L (Figure 11, B and C).

**Discussion**

First reported over a decade ago, WNK bodies were initially described as punctate clusters of the WNK-SPAK/OSR1 pathway that form in the DCT during potassium deficiency (15, 34). Subsequent studies noted that these foci are membraneless, consistent with the notion that they are specialized biomolecular condensates that assemble during potassium stress (12, 18). WNK body formation requires KS-WNK1, but the role of this isoform in DCT salt transport has been elusive. Early in vitro work reported that KS-WNK1 inhibits NCC-mediated sodium transport (35, 36). Subsequent studies in germline global KS-WNK1 knockout mice by Hadchouel *et al.* (28) and Liu *et al.* (37) seemed to corroborate this, as baseline NCC phosphorylation was modestly increased in knockouts compared to controls. More recently, similar results were reported by Ferdaus *et al.* in a conditional DCT-specific KS-WNK1 knockout (29). Despite these observations, other in vitro and in vivo studies have claimed the converse, that KS-WNK1 is an NCC activator (23, 38-40). To complicate matters further, Bahena-Lopez *et al.* recently proposed that KS-WNK1 can function as either an NCC inhibitor or activator depending on dietary potassium intake (23). These apparent contradictions are reconciled when the effect of KS-WNK1 on pNCC is analyzed as a function of blood [$K^+$]. Subjecting over 100 KS-WNK1 KO mice and littermate controls to various potassium maneuvers designed to manipulate NCC phosphorylation across a wide physiologic range, we

found that KS-WNK1 KO mice exhibit reduced pNCC during hypokalemia and increased pNCC relative to WT mice during hyperkalemia. Thus, KS-WNK1 can function as an activator or an inhibitor of NCC, depending on potassium status. Integrating these results as a function of blood [$K^+$] in regression analyses, we found that the steep inverse relationship between NCC phosphorylation and potassium is blunted in KS-WNK1 KO mice. This indicates that KS-WNK1's true function is to expand the dynamic range of NCC phosphorylation across the entire physiologic spectrum of blood potassium concentrations that are experienced during life. In order for the DCT to adjust salt reabsorption in response to potassium imbalance, it must sense small fluctuations in interstitial potassium concentrations and then convert those tiny changes into robust effects on NCC activity. Our findings demonstrate that KS-WNK1 is an essential part of this signal amplification mechanism.

The concept that KS-WNK1 amplifies the DCT's responsiveness to [$K^+$] resolves the apparent discrepancies reported in prior studies of KS-WNK1 KO mice. All the in vivo experiments that reported an inhibitory effect of KS-WNK1 on NCC (23, 28, 29, 37) were conducted in mice with blood potassium concentrations that ranged between 4.33 and 7 mmol/L, while the experiment that reported an activating effect of KS-WNK1 on NCC (23) was carried out in mice with an average blood [$K^+$] of 3.5 mmol/L. Given the flattened pNCC response curve observed in KS-WNK1 knockout mice (Figure 3B, 3E), blood potassium concentrations at the higher end of the spectrum would be associated with KS-WNK1-dependent inhibition, while potassium concentrations at the lower end would be associated with KS-WNK1-mediated activation. Thus, we conclude that the studies revealing KS-WNK1 KO mice having slightly higher pNCC expression compared to WT mice were carried out at a point on the potassium response curve that favors mild KS-WNK1

dependent NCC inhibition. Deleting KS-WNK1 in this physiologic range would be insufficient to cause FHHt. Slight discrepancies in the potassium response curve across studies could be due to a variety of factors, including differences in strain, knockout strategy, sample size, dietary maneuver including the potassium anion (21, 26), sexual dimorphism (41, 42), and circadian effects related to time of sacrifice (43), or technical details related to potassium sampling, or pNCC detection (44).

Though KS-WNK1 augments NCC phosphorylation during hypokalemia and dampens NCC phosphorylation during hyperkalemia, the mechanisms of action are distinct. During $K^+$ loading, the relationship between KS-WNK1 and pNCC changes as the blood potassium concentration rises above 5.6 mmol/L. Above this breakpoint, pNCC abundance decreases dramatically, resulting in a steep negative deflection in slope. Since this feature is not present in KS-WNK1 KO mice, our findings suggest that KS-WNK1 recruits an auxiliary mechanism that promotes NCC dephosphorylation during hyperkalemia, independently of WNK4-SPAK/OSR1 signaling. The process also may be WNK body-independent, as these condensates are not visible in hyperkalemic WT mice. Though the underlying mechanism is not clear, our data imply that KS-WNK1 promotes the action of NCC-specific phosphatases, especially given their established role in NCC dephosphorylation during hyperkalemia (4, 5, 45). Interestingly, Grimm *et al*. (45) recently identified a similar $K^+$ deflection point for protein phosphatase inhibitor-1 (I-1; *PPP1R1A*), an inhibitory subunit of protein phosphatase 1A (PP1A) that is highly expressed in the DCT (5). In their study, potassium supplementation inversely correlated with I-1 protein expression and phosphorylation, thereby reducing I-1's ability to inhibit protein phosphatase 1A (PP1A). PP1A promotes potassium-induced dephosphorylation during hyperkalemia (5, 45). Since KS-WNK1

KO mice exhibited impaired NCC dephosphorylation above the I-1 inflection point, this suggests that KS-WNK1 may contribute to the downregulation of I-1 during hyperkalemia. The mechanism by which this might occur remains unknown and is an area of active research.

A challenge in studying KS-WNK1 in mouse kidney tissue is the inconsistent detection of KS-WNK1 protein in kidney lysates via immunoblots. This issue may arise from low protein expression, difficulties extracting KS-WNK1 from WNK bodies, and cross-reactivity of WNK1 antibodies with KS-WNK1 and L-WNK1. To address this, researchers have employed strategies to increase KS-WNK1 protein abundance while targeting bands absent in KS-WNK1 KO mice (23, 39). While these studies have identified a band, mass spectrometry has yet to confirm it as KS-WNK1. While a similar signal has been observed (albeit inconsistently) under extreme dietary $K^+$ restriction, it is uniformly undetectable in WT mice on control or high $K^+$ diets. Despite this, KS-WNK1 regulates NCC dephosphorylation during high $K^+$ intake, suggesting that the protein is at least lowly expressed (23, 24). Like other drivers of phase transitions, perhaps KS-WNK1 binds partners within active subsaturated low abundance "clusters" (46) that somehow promote phosphatase activity under high $K^+$, high chloride conditions. While the underlying mechanisms remain obscure, the relationship between KS-WNK1 and NCC dephosphorylation remains an intriguing area of research with potential insights into the role of signaling scaffolds as both activators and inhibitors of physiological processes.

Studies in $K^+$ restricted KS-WNK1 5Q mutant mice demonstrate that KS-WNK1 recruits the WNK-SPAK/OSR1 pathway within WNK bodies to facilitate activation of SPAK and trafficking of SPAK to the apical membrane. Similar to other condensates that carry out normal cellular

functions and enhance cellular fitness (47, 48), WNK bodies adopt a spherical morphology and exhibit reversibility, as they dissolve upon restoration of potassium (14, 23). In contrast, the 5Q puncta are non-spherical, suggesting that their material properties and deformability differ from wild-type WNK bodies. Furthermore, they appear to be dysfunctional, as phosphorylated SPAK is unable to leave the 5Q condensed phase and traffic to the DCT apical membrane, where it can engage with and phosphorylate NCC. Collectively these findings indicate that that the 5Q mutant protein forms dysfunctional aggregates that trap the WNK signaling pathway, preventing NCC activation during hypokalemia. The tendency of deleterious mutations to cause condensation-prone proteins to form dysfunctional aggregates with altered in vitro morphology and material properties has been reported previously, notably with the RNA binding protein FUS (49). The KS-WNK1 5Q mutant may behave in a similar manner in vivo to adversely affect potassium homeostasis.

The molecular basis by which WNK body condensates augment WNK-SPAK/OSR1 pathway activity remains unresolved; however, our results suggests that normal KS-WNK1 exon 4a structure is required to coordinate optimal SPAK activation. Based on AlphaFold predictions (Figure 9B), we propose that the 5Q mutation disrupts an N-terminal alpha helix but maintains a functional C-terminal IDR that can phase separate and bind WNK body constituents, including L-WNK1, WNK4, and SPAK (12, 14). Like other poly-Q peptides (50), the stretch of consecutive N-terminal glutamines introduced by the 5Q mutation may promote the sequestration, aggregation, and diffusional arrest of KS-WNK1 binding partners, causing the protein to function like a sponge that inhibits signal transduction despite an increase in protein abundance (as suggested by increased SPAK protein abundance)(Figure 10A). Definitive testing of this hypothesis will require

characterization of the material properties of WNK bodies versus 5Q assemblies, both in vivo and in vitro.

Our results also identify KS-WNK1-dependent WNK bodies as key determinants of sex-based differences in distal nephron function. Our data suggest that female mice require DCT WNK bodies to minimize salt wasting and maintain potassium homeostasis. Recent observations indicate that females prioritize distal tubule salt reabsorption via NCC more than males (41, 51). The reason for this is unclear, but a role for NCC in defending against hypokalemia during pregnancy has been proposed (52). Regardless, our data suggest that the underlying mechanism is dependent on the ability of females to leverage the distal tubule and WNK body-mediated signaling more efficiently during the threat of potassium deficiency. Given the influence on whole animal physiology, our findings more generally imply that biomolecular condensates may contribute to sexual dimorphism in other regulatory systems.

Lastly, our results from normal human kidney parenchyma, reveal an inverse relationship between WNK body condensate abundance that progressively increased as $[K^+]$ fell below 4.0 mmol/L. This mimics the inverse relationship observed in mice between $[K^+]$ and WNK body expression. Due to a limited number of humans tissue samples, we were unable to probe for pSPAK and/or pNCC activation. Nevertheless, Thompson *et al*. have previously shown in human kidney tissue from patients with severe hypokalemia that there is an increase in WNK body abundance that correlates with an increase in pSPAK at the apical membrane (16). In addition, studies have demonstrated an inverse relationship between dietary potassium intake and pNCC in human urinary exosomes (53). Taken together, these studies suggest that in humans, WNK bodies are

involved in activation of the WNK-SPAK/OSR1 pathway—not just during frank hypokalemia, but also when blood potassium concentrations are in the low-normal reference range of 3.5-4.0 mmol/L. This raises an intriguing question about the current laboratory definition of normokalemia—is a [$K^+$] of 3.5 mmol/L truly "normal" if it is sufficient to induce a stress response that promotes WNK body formation, which would predispose to blood pressure salt-sensitivity? Indeed, a recent meta-analysis comprising greater than 1 million participants found that the risk of adverse cardiovascular outcomes, end stage kidney disease, and all-cause mortality increases as blood [$K^+$] falls below 4.0 mmol/L (54). Conceivably, titrating $K^+$ intake to achieve a plasma potassium concentration sufficient to inhibit WNK body condensation may be an effective natriuretic antihypertensive strategy in certain clinical scenarios (55-57).

In conclusion, our findings provide insight into the role of KS-WNK1 and WNK body condensates in potassium-dependent NCC regulation in both mice and humans. They identify KS-WNK1 as a DCT-specific amplifier that optimizes NCC reactivity to changes in systemic potassium concentrations. This observation reconciles almost two decades of conflicting data regarding stimulatory vs inhibitory effects of KS-WNK1 on NCC. Key to the amplification process is KS-WNK1's ability to organize the WNK signaling pathway within specialized biomolecular condensates that impact potassium metabolism, blood pressure salt sensitivity, and nephron sexual dimorphism. WNK body assembly requires KS-WNK1, which emerged during vertebrate kidney evolution from L-WNK1, a crowding-sensitive condensation-prone protein that first appeared in single celled organisms to control salt transport and fluid volume (17, 18). Thus, it appears that through nephron segment-specific isoform expression, the mammalian kidney repurposed this

ancient condensate-dependent volume regulatory system for total body potassium and blood pressure homeostasis.

## Methods

*Sex as a biological variable*

Our study disaggregated data from male and female animals, and sexual-dimorphic effects are reported.

*Mice*

KS-WNK1 knockout mice **(**KS-WNK1 KO) and age-matched wild-type littermates (WT) were generated in a 129/Sv background as previously described (12, 37). For the generation of the KS-WNK1 "5Q" mutant mice in a 129/Sv background CRISPR-Cas9 homology-directed repair was used to knock-in a mutation in exon 4a of the *WNK1* gene, replacing five consecutive bulky hydrophobic residues (spanning Val-11 to Val-15) with five neutral glutamines (Figure 9A, S8, A-D). Please see supplemental methods for more detailed information.

*Dietary Maneuvers*

To determine the effect of KS-WNK1 on NCC phosphorylation, mice were fed $K^+$ diets for 10 days: (1) low $K^+$, (2) control $K^+$, (3) high $K^+$ basic, (4) high KCl (Teklad). To induce hyperkalemia, mice fed the high $K^+$ basic diet were supplemented with amiloride (2mg/kg/d) in their drinking water for 10d. To measure the effect of KS-WNK1 on intake, output, and blood and urine parameters, mice were individually housed in metabolic cages (Tecniplast). After 10d, mice were anesthetized with isoflurane, and blood was obtained via terminal cardiac puncture and analyzed by iSTAT (Abbot). Kidneys were harvested and flash frozen for immunoblot and/or paraformaldehyde-treated for microscopy. Further details can be found in supplemental methods.

*Immunohistochemistry*

In accordance with the University of Pittsburgh Internal Review Board (IRB: STUDY19120038) the Pitt Biospecimen Core provided formalin-fixed, paraffin-embedded non-neoplastic kidney tissue from 6 subjects who underwent radical nephrectomy for renal tumors (Figure 11). For processing and imaging information please see supplemental methods.

*Immunoblotting*

For protein quantification, mouse kidney cortexes were flash frozen and processed as previously described (21) and further described in supplemental methods. Uniform protein loading was determined using Coomassie-stained gels, as previously described (21, 44). Next, equal amounts (20-40µg) of protein were separated by SDS-PAGE using 4-20% Criterion TGX precast gels (Bio-Rad). Protein was transferred to a nitrocellulose membrane. Signal densitometry was measured using Bio-Rad ChemiDoc and densitometry was quantified with ImageLab analysis software (Bio-Rad). To plot NCC densitometry values as a function of blood $[K^+]$, WT and mutant mice placed on control diets were run on the same gel as WT and mutant mice treated with a specific potassium maneuver (Figure S2). This permitted normalization of all values to the protein abundance in WT mice on control diet. Antibodies are listed in supplemental methods.

*Blood Pressure Telemetry*

Female KS-WNK1 KO mice and WT littermates were anesthetized with isoflurane and DSI PA-C10 telemetry units (Data Sciences International) were surgically implanted into the femoral artery as previously described (58). Blood pressure was collected every day from 10am-4pm (daytime)

and 10pm-4am (nighttime) for the duration of the diet challenge using Spike2 software (Cambridge Electronic Design). HCTZ-challenge was performed on day 15. During the HCTZ treatment mice were maintained on either control or low K+ diet with 1% saline drinking water. Daytime blood pressure was obtained for 6h the day prior to HCTZ administration and on the day of HCTZ administration. Mice were injected with hydrochlorothiazide (25mg/kg IP) at 9am and then blood pressure was collected from 10am-4pm (daytime). For more details see supplemental methods.

*Diuretic Challenge*

Mice were placed on respective $K^+$ diets for 10 days. For the first 8 days they were housed in the standard cages. On day 9 they were individually housed in metabolic cages and acclimated for 24h. On day 10 mice were given intraperitoneal injections of hydrochlorothiazide (HCTZ; 25mg/kg) and urine was collected for 6 hours. Urine [$Na^+$], [$K^+$], and [$Cl^-$] were determined using Easy Lyte Plus Na/K/Cl analyzer (Medica Corp).

*Quantitative Immunofluorescence Confocal Microscopy*

For Figure 4, WNK body analysis and quantification in formalin-fixed, paraffin-embedded mouse kidney, tissues sectioned at 5-µm thickness were processed for immunofluorescence staining according to a protocol similar to the immunohistochemistry protocol used for human tissue described above and further details in supplemental figure. Images were acquired with a Leica DM6000B widefield microscope with a Retiga 4000R Fast 1394 camera. Two independent, blinded analyses were conducted to measure WNK body size and count using a custom macro in ImageJ. The results were averaged, unblinded, and plotted as a function of blood [$K^+$].

For Figures 6 and 9, Paraformaldehyde fixed kidney tissues were processed and prepared as previously described (21) and further described in supplemental methods. Imaging of the kidney tissue was performed using a Leica HCX PL APO CS x40, 1.25 numerical aperture oil objective on a Leica TCS SP5 CW-STED confocal microscope utilizing Leica LAS-X software. To produce quantitative measures for pSPAK/pOSR1 puncta number, size, and distance to the DCT lumen we used Imaris (Bitplane, v9.5) image analysis software as described in supplemental methods. To measure WNK condensate morphology in 5Q mice (Figure 9), confocal images of WNK1 signal from WT and KS-WNK1 5Q mice were obtained under identical confocal settings. Images were thresholded under identical parameters to generate masks, which were then used to measure the area and roundness of individual puncta, using the "Analyze Particles" tool in FIJI.

*CLEM*

Correlative Light and Electron Microscopy (CLEM) was performed using an innovative approach pairing high resolution fluorescence imaging with immunogold labelling and backscattered scanning electron (BSE) detection via scanning electron microscopy (SEM) of 300nm semithin frozen sections (Figure 4). Sections were labelled with primary antibodies to WNK1 revealed with secondary antibodies labelled with a dual 5nm gold/alexa 488 conjugate. Sections were scanned *in toto* using high resolution fluorescence microscopy using a Nikon Ti microscope, with a 100x 1.49 objective and Photometrics 95B camera (effective pixel size =0.07um). The sections were then counterstained with heavy metals (OsO4, Pb citrate and Ua) critical point dried and carbon coated prior to mounting the same coverslips imaged by light microscopy in a JEOL SEM. Following a low magnification SEM scan using backscattered electron detection, the image was inverted and overlaid with the fluorescent image. This was used to guide nanometer resolution ultra structural

identification of WNK bodies. In these inverted EM images, dark signal corresponds to regions of high material density. Further details in supplemental methods.

*Protein structure prediction*

The amino-terminal structures of WT and 5Q mutant KS-WNK1 (residues 1-72, encompassing exon 4a to the C-terminal end of the remnant kinase domain; residue 494 of Uniprot sequence Q9JIH7-1) were predicted using ColabFold (59), accessed via UCSF ChimeraX (60). Full-length L- and KS-WNK1 were rendered with AlphaFold3 (61).

*Statistics*

Data were analyzed using GraphPad Prism software and presented as mean ± SE, plus individual data points. Comparisons between two groups were determined by a Student's T-test. Comparisons between multiple groups were determined using one- or two-way analysis of variance (ANOVA), followed by the appropriate post hoc test, as indicated. P values $\leq 0.05$ were considered statistically significant. To analyze the relationship between blood $[K^+]$ and NCC, regression analyses were performed in Prism. Data were preliminarily fitted via one phase decay, indicating an exponential relationship with suboptimal goodness of fit. Thus, the absolute Y-values (representing normalized protein densitometry as described above) were logarithmically transformed and analyzed by segmental vs simple linear regression. A comparison of fits was performed by F-test, with data presented fit to the preferred regression model (alternative hypothesis = segmental vs null hypothesis = straight line). P values for these comparisons are shown with the corresponding residuals in Figure S5.

*Study Approval*

Animal Studies. All animal protocols conform to the National Institutes of Health (NIH) Guide for the Care and Use of Laboratory Animals and were approved by the University of Pittsburgh IACUC.

Human Studies. All research was approved by the University of Pittsburgh Internal Review Board (IRB) as exemption for secondary research with data and /or specimens (IRB: STUDY19120038). An IRB-approved Honest Broker provided the de-identified, safe harbor data including age, sex, and serum $K^+$ measured on the day of surgery.

*Data Availability*

Raw and analyzed data are included in the accompanying Supporting Data Values file. Any additional information required to reanalyze the data reported in this paper is available from the corresponding author upon request.

## Author Contributions

C.B.S. and A.R.S. designed the study; C.B.S, R.T.B., J.A.L., M.N.V., A.B, S.A.K., S.E.G., L.J.N., K.Q., A.L.M., J.F., M.S., S.C.W, and S.D.S. performed experiments; C.B.S., D.J.S., M.N.V., N.H.N, A.B, S.D.S., S.A.K., S.C.W., O.B.K., and A.R.S. analyzed data; C.B.S., D.J.S., and A.R.S. made figures; C.B.S., R.T.B., S.E.G., D.J.S., S.C.W., A.R.R., S.D.S., O.B.K., and A.R.S. drafted the paper; C-L.H. provided KS-WNK1 knockout mice; all authors approved the final version of the manuscript.

## Acknowledgments

We thank Tom Kleyman for helpful discussions. This work was supported by National Institutes of Health grants K08DK118211 (to C.B.S), R03DK138215 (to C.B.S.), R00HL155777 (to D.J.S.), R01DK098145 (to A.R.S. and A.R.R.), R01DK119252 (to A.R.S.), R01DK110358 (to A.R.R.), R01HL145875 (to S.D.S), R01HL152680 (to S.D.S.), R01DK111542 (to C-L.H.), R01DK125439 (to O.B.K.), S10OD021627, S10OD028596, P30DK79307, & U54DK137329 (Pittsburgh Center for Kidney Research), S10OD036205 (to S.C.W), and a Carl W. Gottschalk Research Scholar of KidneyCure Award (to C.B.S.). This content is solely the responsibility of authors and does not necessarily represent the views of the U.S. Department of Veterans Affairs.

## Declaration of Interests

The authors have declared no conflict of interest exits.

## References


1. Boyd-Shiwarski CR, and Subramanya AR. The renal response to potassium stress: integrating past with present. *Curr Opin Nephrol Hypertens.* 2017;26(5):411-8.

2. Terker AS, Zhang C, McCormick JA, Lazelle RA, Zhang C, Meermeier NP, et al. Potassium modulates electrolyte balance and blood pressure through effects on distal cell voltage and chloride. *Cell metabolism.* 2015;21(1):39-50.

3. Hoorn EJ, Gritter M, Cuevas CA, and Fenton RA. Regulation of the Renal NaCl Cotransporter and Its Role in Potassium Homeostasis. *Physiol Rev.* 2020;100(1):321-56.

4. Sorensen MV, Grossmann S, Roesinger M, Gresko N, Todkar AP, Barmettler G, et al. Rapid dephosphorylation of the renal sodium chloride cotransporter in response to oral potassium intake in mice. *Kidney Int.* 2013;83(5):811-24.

5. Picard N, Trompf K, Yang CL, Miller RL, Carrel M, Loffing-Cueni D, et al. Protein phosphatase 1 inhibitor-1 deficiency reduces phosphorylation of renal NaCl cotransporter and causes arterial hypotension. *Journal of the American Society of Nephrology : JASN.* 2014;25(3):511-22.

6. Terker AS, Zhang C, Erspamer KJ, Gamba G, Yang CL, and Ellison DH. Unique chloride-sensing properties of WNK4 permit the distal nephron to modulate potassium homeostasis. *Kidney Int.* 2016;89(1):127-34.

7. Wilson FH, Disse-Nicodeme S, Choate KA, Ishikawa K, Nelson-Williams C, Desitter I, et al. Human hypertension caused by mutations in WNK kinases. *Science.* 2001;293(5532):1107-12.

8. Subramanya AR, and Ellison DH. Distal convoluted tubule. *Clin J Am Soc Nephrol.* 2014;9(12):2147-63.

9. Takahashi D, Mori T, Nomura N, Khan MZ, Araki Y, Zeniya M, et al. WNK4 is the major WNK positively regulating NCC in the mouse kidney. *Biosci Rep.* 2014;34(3).

10. Vidal-Petiot E, Cheval L, Faugeroux J, Malard T, Doucet A, Jeunemaitre X, et al. A new methodology for quantification of alternatively spliced exons reveals a highly tissue-specific expression pattern of WNK1 isoforms. *PLoS One.* 2012;7(5):e37751.

11. Delaloy C, Lu J, Houot AM, Disse-Nicodeme S, Gasc JM, Corvol P, et al. Multiple promoters in the WNK1 gene: one controls expression of a kidney-specific kinase-defective isoform. *Mol Cell Biol.* 2003;23(24):9208-21.

12. Boyd-Shiwarski CR, Shiwarski DJ, Roy A, Namboodiri HN, Nkashama LJ, Xie J, et al. Potassium-regulated distal tubule WNK bodies are kidney-specific WNK1 dependent. *Mol Biol Cell.* 2018;29(4):499-509.

13. Wang XP, Balchak DM, Gentilcore C, Clark NL, and Kashlan OB. Activation by cleavage of the epithelial Na(+) channel alpha and gamma subunits independently coevolved with the vertebrate terrestrial migration. *Elife.* 2022;11.

14. Thomson MN, Cuevas CA, Bewarder TM, Dittmayer C, Miller LN, Si J, et al. WNK bodies cluster WNK4 and SPAK/OSR1 to promote NCC activation in hypokalemia. *Am J Physiol Renal Physiol.* 2020;318(1):F216-F28.

15. Grimm PR, Taneja TK, Liu J, Coleman R, Chen YY, Delpire E, et al. SPAK isoforms and OSR1 regulate sodium-chloride co-transporters in a nephron-specific manner. *J Biol Chem.* 2012;287(45):37673-90.

16. Thomson MN, Schneider W, Mutig K, Ellison DH, Kettritz R, and Bachmann S. Patients with hypokalemia develop WNK bodies in the distal convoluted tubule of the kidney. *Am J Physiol Renal Physiol.* 2019;316(2):F292-F300.

17. Boyd-Shiwarski CR, Shiwarski DJ, Griffiths SE, Beacham RT, Norrell L, Morrison DE, et al. WNK kinases sense molecular crowding and rescue cell volume via phase separation. *Cell.* 2022;185(24):4488-506 e20.

18. Boyd-Shiwarski CR, Shiwarski DJ, and Subramanya AR. A New Phase for WNK Kinase Signaling Complexes as Biomolecular Condensates. *Physiology (Bethesda).* 2024.

19. Xiao YX, Lee SY, Aguilera-Uribe M, Samson R, Au A, Khanna Y, et al. The TSC22D, WNK, and NRBP gene families exhibit functional buffering and evolved with Metazoa for cell volume regulation. *Cell Rep.* 2024;43(7):114417.

20. Subramanya AR, and Boyd-Shiwarski CR. Molecular Crowding: Physiologic Sensing and Control. *Annu Rev Physiol.* 2024;86:429-52.

21. Boyd-Shiwarski CR, Weaver CJ, Beacham RT, Shiwarski DJ, Connolly KA, Nkashama LJ, et al. Effects of extreme potassium stress on blood pressure and renal tubular sodium transport. *Am J Physiol Renal Physiol.* 2020;318(6):F1341-F56.

22. Richardson C, Rafiqi FH, Karlsson HK, Moleleki N, Vandewalle A, Campbell DG, et al. Activation of the thiazide-sensitive Na+-Cl- cotransporter by the WNK-regulated kinases SPAK and OSR1. *J Cell Sci.* 2008;121(Pt 5):675-84.

23. Bahena-Lopez JP, Vergara L, De la Pena V, Gutierrez-Gallardo MA, Lopez-Ibarguen P, Garcia JA, et al. KS-WNK1 is Required for the Renal Response to Extreme Changes in Potassium Intake. *Am J Physiol Renal Physiol.* 2024.

24. Wu P, Gao ZX, Su XT, Ellison DH, Hadchouel J, Teulon J, et al. Role of WNK4 and kidney-specific WNK1 in mediating the effect of high dietary K(+) intake on ROMK channel in the distal convoluted tubule. *Am J Physiol Renal Physiol.* 2018;315(2):F223-F30.

25. Rastegar A. In: Walker HK, Hall WD, and Hurst JW eds. *Clinical Methods: The History, Physical, and Laboratory Examinations*. Boston; 1990.

26. Castaneda-Bueno M, Cervantes-Perez LG, Rojas-Vega L, Arroyo-Garza I, Vazquez N, Moreno E, et al. Modulation of NCC activity by low and high K(+) intake: insights into the signaling pathways involved. *Am J Physiol Renal Physiol.* 2014;306(12):F1507-19.

27. Penton D, Czogalla J, Wengi A, Himmerkus N, Loffing-Cueni D, Carrel M, et al. Extracellular K(+) rapidly controls NaCl cotransporter phosphorylation in the native distal convoluted tubule by Cl(-) -dependent and independent mechanisms. *J Physiol.* 2016;594(21):6319-31.

28. Hadchouel J, Soukaseum C, Busst C, Zhou XO, Baudrie V, Zurrer T, et al. Decreased ENaC expression compensates the increased NCC activity following inactivation of the kidney-specific isoform of WNK1 and prevents hypertension. *Proc Natl Acad Sci U S A.* 2010;107(42):18109-14.

29. Ferdaus MZ, Terker AS, Koumangoye RB, Al-Qusairi L, Welling PA, and Delpire E. Deletion of KS-WNK1 promotes NCC activation by increasing WNK1/4 abundance. *Am J Physiol Renal Physiol.* 2024;327(3):F373-F85.

30. Lazrak A, Liu Z, and Huang CL. Antagonistic regulation of ROMK by long and kidney-specific WNK1 isoforms. *Proc Natl Acad Sci U S A.* 2006;103(5):1615-20.

31. Wade JB, Fang L, Liu J, Li D, Yang CL, Subramanya AR, et al. WNK1 kinase isoform switch regulates renal potassium excretion. *Proc Natl Acad Sci U S A.* 2006;103(22):8558-63.

32. Cheng CJ, Baum M, and Huang CL. Kidney-specific WNK1 regulates sodium reabsorption and potassium secretion in mouse cortical collecting duct. *Am J Physiol Renal Physiol.* 2013;304(4):F397-402.

33. Bettinelli A, Vezzoli G, Colussi G, Bianchetti MG, Sereni F, and Casari G. Genotype-phenotype correlations in normotensive patients with primary renal tubular hypokalemic metabolic alkalosis. *J Nephrol.* 1998;11(2):61-9.

34. McCormick JA, Mutig K, Nelson JH, Saritas T, Hoorn EJ, Yang CL, et al. A SPAK isoform switch modulates renal salt transport and blood pressure. *Cell metabolism.* 2011;14(3):352-64.

35. Subramanya AR, Yang CL, Zhu X, and Ellison DH. Dominant-negative regulation of WNK1 by its kidney-specific kinase-defective isoform. *Am J Physiol Renal Physiol.* 2006;290(3):F619-24.

36. Yang CL, Zhu X, and Ellison DH. The thiazide-sensitive Na-Cl cotransporter is regulated by a WNK kinase signaling complex. *J Clin Invest.* 2007;117(11):3403-11.

37. Liu Z, Xie J, Wu T, Truong T, Auchus RJ, and Huang CL. Downregulation of NCC and NKCC2 cotransporters by kidney-specific WNK1 revealed by gene disruption and transgenic mouse models. *Hum Mol Genet.* 2011;20(5):855-66.

38. Argaiz ER, Chavez-Canales M, Ostrosky-Frid M, Rodriguez-Gama A, Vazquez N, Gonzalez-Rodriguez X, et al. Kidney-specific WNK1 isoform (KS-WNK1) is a potent activator of WNK4 and NCC. *Am J Physiol Renal Physiol.* 2018;315(3):F734-F45.

39. Ostrosky-Frid M, Chavez-Canales M, Zhang J, Andrukhova O, Argaiz ER, Lerdo-de-Tejada F, et al. Role of KLHL3 and dietary K(+) in regulating KS-WNK1 expression. *Am J Physiol Renal Physiol.* 2021;320(5):F734-F47.

40. Louis-Dit-Picard H, Kouranti I, Rafael C, Loisel-Ferreira I, Chavez-Canales M, Abdel-Khalek W, et al. Mutation affecting the conserved acidic WNK1 motif causes inherited hyperkalemic hyperchloremic acidosis. *J Clin Invest.* 2020.

41. Veiras LC, Girardi ACC, Curry J, Pei L, Ralph DL, Tran A, et al. Sexual Dimorphic Pattern of Renal Transporters and Electrolyte Homeostasis. *Journal of the American Society of Nephrology : JASN.* 2017;28(12):3504-17.

42. Rojas-Vega L, Reyes-Castro LA, Ramirez V, Bautista-Perez R, Rafael C, Castaneda-Bueno M, et al. Ovarian hormones and prolactin increase renal NaCl cotransporter phosphorylation. *Am J Physiol Renal Physiol.* 2015;308(8):F799-808.

43. Ivy JR, Jones NK, Costello HM, Mansley MK, Peltz TS, Flatman PW, et al. Glucocorticoid receptor activation stimulates the sodium-chloride cotransporter and influences the diurnal rhythm of its phosphorylation. *Am J Physiol Renal Physiol.* 2019;317(6):F1536-F48.

44. McDonough AA, Veiras LC, Minas JN, and Ralph DL. Considerations when quantitating protein abundance by immunoblot. *Am J Physiol Cell Physiol.* 2015;308(6):C426-33.

45. Grimm PR, Tatomir A, Rosenbaek LL, Kim BY, Li D, Delpire EJ, et al. Dietary potassium stimulates Ppp1Ca-Ppp1r1a dephosphorylation of kidney NaCl co-transporter and reduces blood pressure. *J Clin Invest.* 2023.

46. Kar M, Dar F, Welsh TJ, Vogel LT, Kuhnemuth R, Majumdar A, et al. Phase-separating RNA-binding proteins form heterogeneous distributions of clusters in subsaturated solutions. *Proc Natl Acad Sci U S A.* 2022;119(28):e2202222119.

47. Shin Y, and Brangwynne CP. Liquid phase condensation in cell physiology and disease. *Science.* 2017;357(6357).

48. Franzmann TM, Jahnel M, Pozniakovsky A, Mahamid J, Holehouse AS, Nuske E, et al. Phase separation of a yeast prion protein promotes cellular fitness. *Science.* 2018;359(6371).

49. Patel A, Lee HO, Jawerth L, Maharana S, Jahnel M, Hein MY, et al. A Liquid-to-Solid Phase Transition of the ALS Protein FUS Accelerated by Disease Mutation. *Cell.* 2015;162(5):1066-77.

50. Wetzel R. Physical chemistry of polyglutamine: intriguing tales of a monotonous sequence. *J Mol Biol.* 2012;421(4-5):466-90.

51. Tahaei E, Coleman R, Saritas T, Ellison DH, and Welling PA. Distal convoluted tubule sexual dimorphism revealed by advanced 3D imaging. *Am J Physiol Renal Physiol.* 2020;319(5):F754-F64.

52. McDonough AA, and Layton AT. Sex differences in renal electrolyte transport. *Curr Opin Nephrol Hypertens.* 2023;32(5):467-75.

53. Ellison DH, and Terker AS. Why Your Mother Was Right: How Potassium Intake Reduces Blood Pressure. *Trans Am Clin Climatol Assoc.* 2015;126:46-55.

54. Kovesdy CP, Matsushita K, Sang Y, Brunskill NJ, Carrero JJ, Chodick G, et al. Serum potassium and adverse outcomes across the range of kidney function: a CKD Prognosis Consortium meta-analysis. *Eur Heart J.* 2018;39(17):1535-42.

55. Chan RJ, Parikh N, Ahmed S, Ruzicka M, and Hiremath S. Blood Pressure Control Should Focus on More Potassium: Controversies in Hypertension. *Hypertension (Dallas, Tex : 1979).* 2024;81(3):501-9.

56. Neal B, Wu Y, Feng X, Zhang R, Zhang Y, Shi J, et al. Effect of Salt Substitution on Cardiovascular Events and Death. *N Engl J Med.* 2021;385(12):1067-77.

57. Sriperumbuduri S, Welling P, Ruzicka M, Hundemer GL, and Hiremath S. Potassium and Hypertension: A State-of-the-Art Review. *Am J Hypertens.* 2024;37(2):91-100.

58. Ong J, Kinsman BJ, Sved AF, Rush BM, Tan RJ, Carattino MD, et al. Renal sensory nerves increase sympathetic nerve activity and blood pressure in 2-kidney 1-clip hypertensive mice. *J Neurophysiol.* 2019;122(1):358-67.

59. Mirdita M, Schutze K, Moriwaki Y, Heo L, Ovchinnikov S, and Steinegger M. ColabFold: making protein folding accessible to all. *Nat Methods.* 2022;19(6):679-82.

60. Meng EC, Goddard TD, Pettersen EF, Couch GS, Pearson ZJ, Morris JH, et al. UCSF ChimeraX: Tools for structure building and analysis. *Protein Sci.* 2023;32(11):e4792.

61. Abramson J, Adler J, Dunger J, Evans R, Green T, Pritzel A, et al. Accurate structure prediction of biomolecular interactions with AlphaFold 3. *Nature.* 2024;630(8016):493-500.

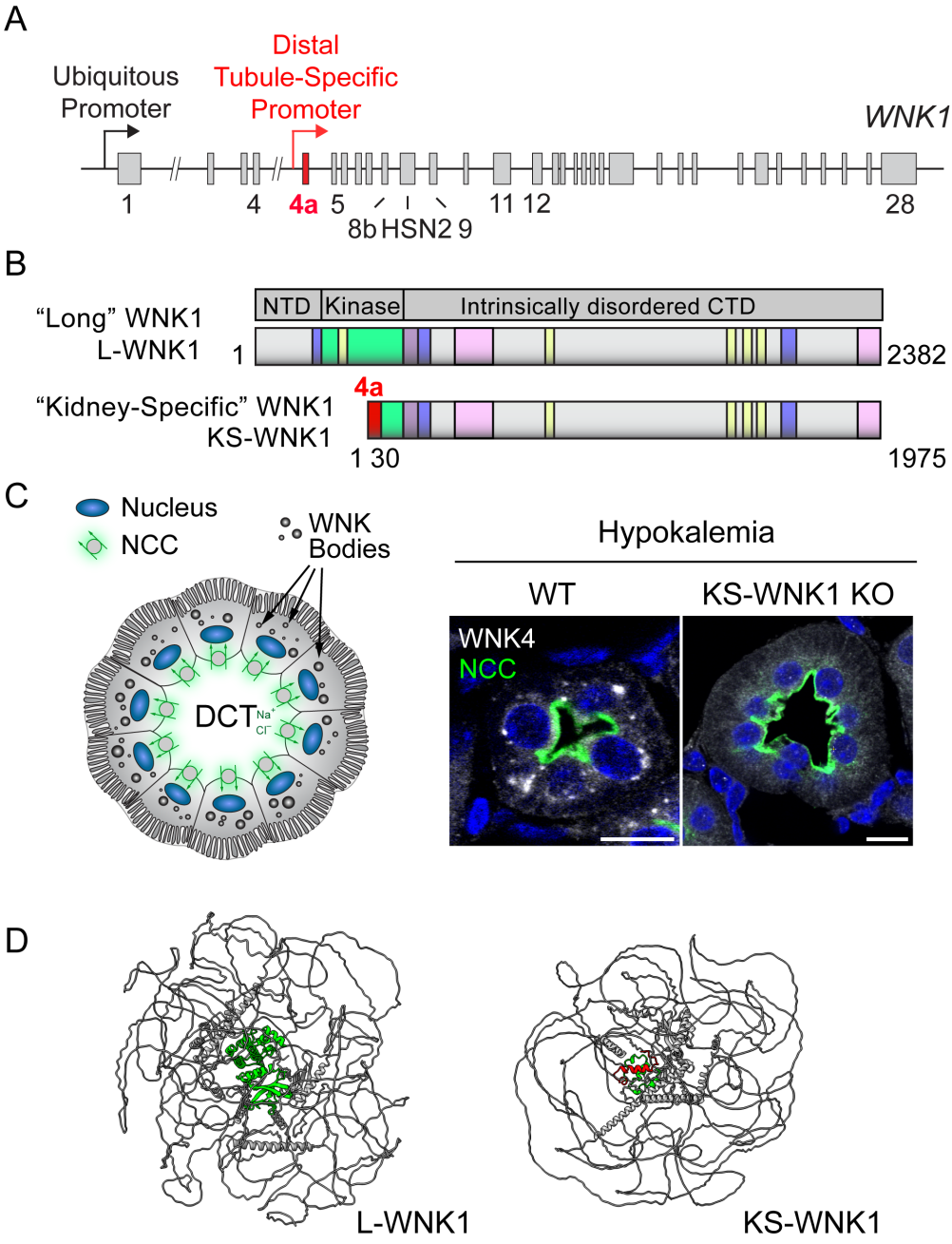


**Figure 1. KS-WNK1 is a DCT-specific disordered protein that drives WNK body condensate formation**
**(A)** Schematic representation of the *WNK1* gene. A ubiquitously expressed promoter drives L-WNK1 transcription. A distal tubule-specific promoter drives the expression of the truncated KS-WNK1 isoform. **(B)** Domain architecture of L- and KS-WNK1 isoforms. Full-length "long" WNK1 contains an N-terminal domain (NTD), a serine-threonine kinase domain (green), and a >100kDa intrinsically disordered C-terminal domain (CTD) that drives condensate formation(17). Other functional signatures include SPAK/OSR1 binding motifs (yellow), coiled-coil domains (purple), and prion-like regions (pink). KS-WNK1 lacks the NTD and most of the kinase domain, replaced by a 30AA sequence encoded by exon 4a (red). Schematics adapted with permission from Boyd-Shiwarski et al(12). **(C)** Illustration (left) and immunofluorescence (IF) staining (right) of WNK bodies, which form in NCC-expressing DCT cells during hypokalemia. KS-WNK1 KO mice fail to form WNK bodies. Bar=10µm. **(D)** Alphafold3 predictions of L-WNK1 and KS-WNK1, highlighting their extensive disorder. Green structured region in L-WNK1 is the kinase domain, red structured region in KS-WNK1 is exon 4a.

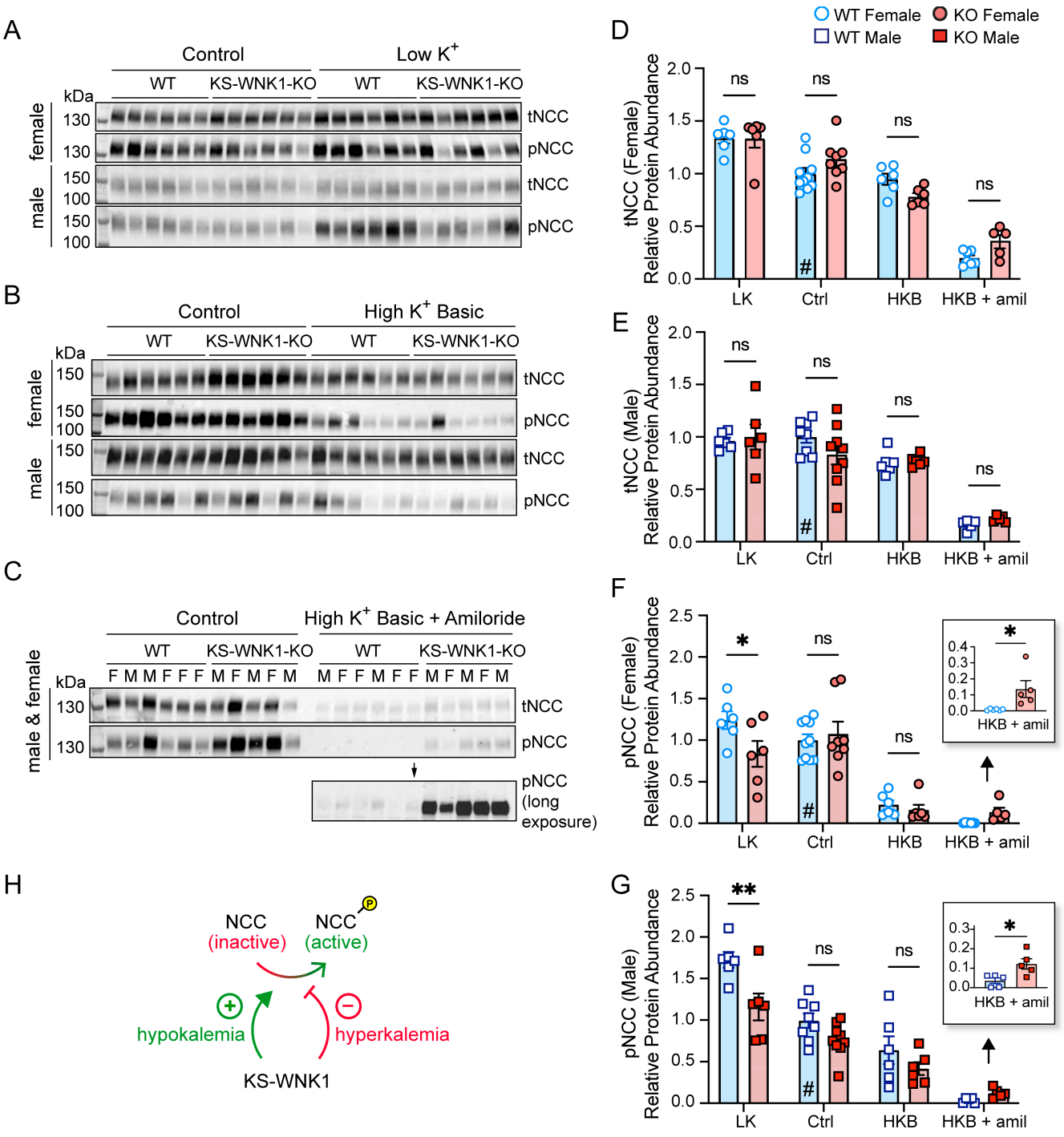


**Figure 2. KS-WNK1 differentially alters NCC abundance and phosphorylation during hypo- and hyperkalemia.** **(A-C)** Immunoblot (IB) analysis of kidney cortical extracts from female and male WT littermates and KS-WNK1 KO mice subjected to 10d maneuvers that alter $K^+$ homeostasis. Immunoblots of total NCC (tNCC) and active phospho Thr53 NCC (pNCC), from female and male mice fed either control diet (Ctrl) versus: **(A)** low $K^+$ diet (LK), **(B)** high $K^+$ basic diet (HKB), or **(C)** high $K^+$ basic + amiloride (HKB + amil) (2mg/kg/day). In A and B, lanes corresponding to WT and KO animals on control diet were from replicate lysates to facilitate normalization between blots. The average from these replicates were plotted for control diet (see Figure S2). Additional values for WT and KO mice on control diet were obtained from Figure 2C. **(D-E)** KS-WNK1 had no significant effect on tNCC abundance, regardless of sex. **(F-G)** KS-WNK1 had significant effects on pNCC during LK and HKB+amiloride. **(H)** These data indicate that KS-WNK1 stimulates NCC during hypokalemia and inhibits during hyperkalemia. Results are shown as means ± SE; $n$ = 5-6 mice per genotype, sex, and diet, except control diet $n$ = 8-10 mice. M = male, F = female. Two-way ANOVA with Sidak's multiple comparisons test, $*P \leq 0.05$, $**P \leq 0.01$. For **D-G**, data were normalized to WT mice on control diet, indicated by #.

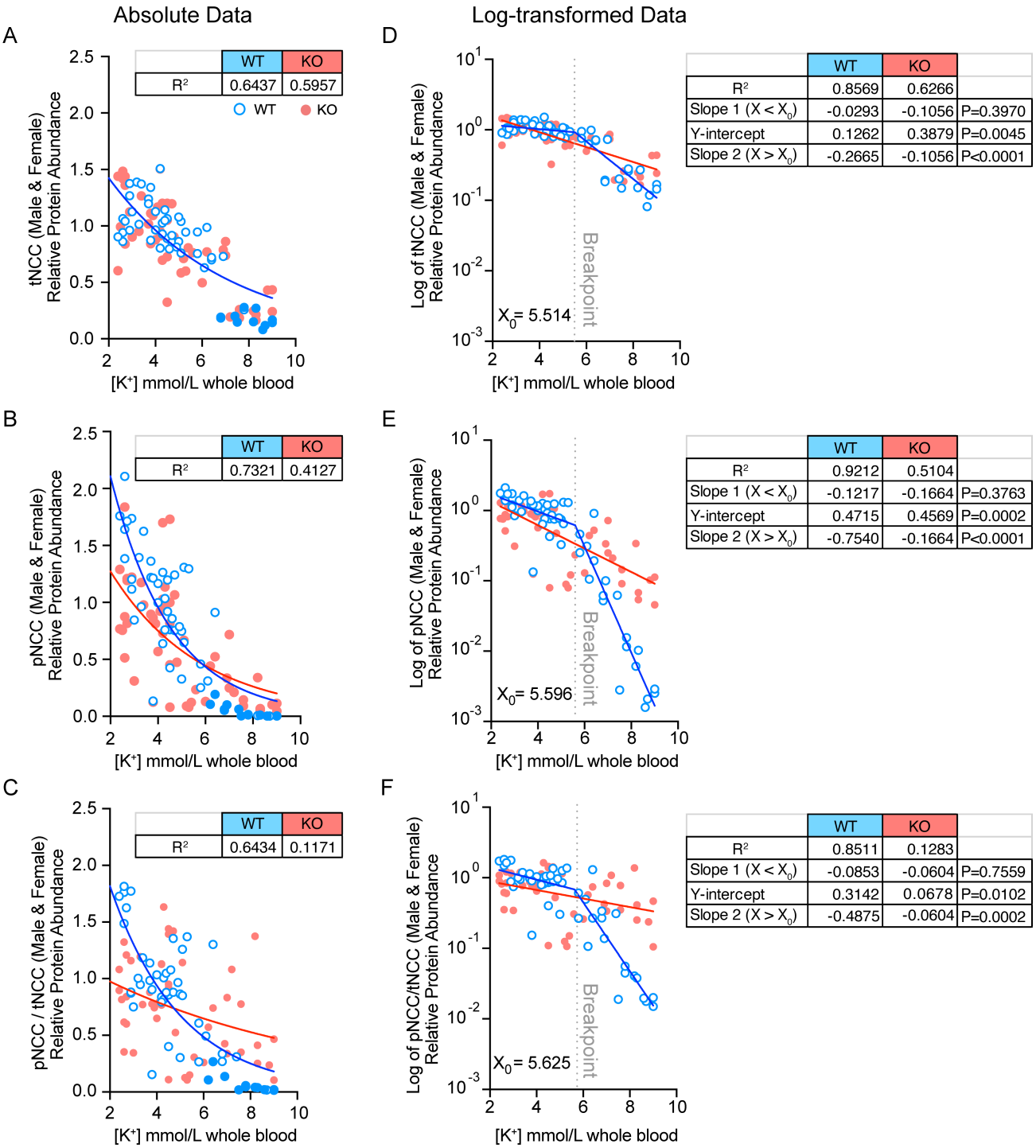


**Figure 3. KS-WNK1 amplifies the inverse relationship between NCC phosphorylation and blood [K$^+$].**
Total and phosphorylated NCC protein abundance in KS-WNK1 KO (red) versus WT (blue) mice, plotted as a function of blood [K$^+$]. **(A-C)** tNCC, pNCC, and pNCC /tNCC ratio, fit to single exponential curves. $R^2$ measures are presented in table format alongside the graphs. For all graphs, the single exponential function adequately fit the WT data at [K$^+$] < 4.0, but overestimated data points at [K$^+$] >6.0 (filled blue circles). **(D-F)** Normalized tNCC, pNCC, and pNCC/tNCC densitometry in A-C were log transformed and analyzed by linear regression. In all cases, WT data were best fit by a segmented linear regression regime, with $X_0$ breakpoints (dotted line) around 5.6 mmol/L. Slopes of the two linear components are presented in table format alongside the corresponding graphs. For KO mice, Slopes 1 ($X<X_0$) and 2 ($X>X_0$) did not differ as the log-transformed data were best fit by simple linear regression. *P*-values represent slope comparisons between WT and KO; since Slope 1 comparisons did not reach significance, Y-intercept comparisons with *P*-values are shown. See also Figure S5 for results disaggregated by sex and residual plots.

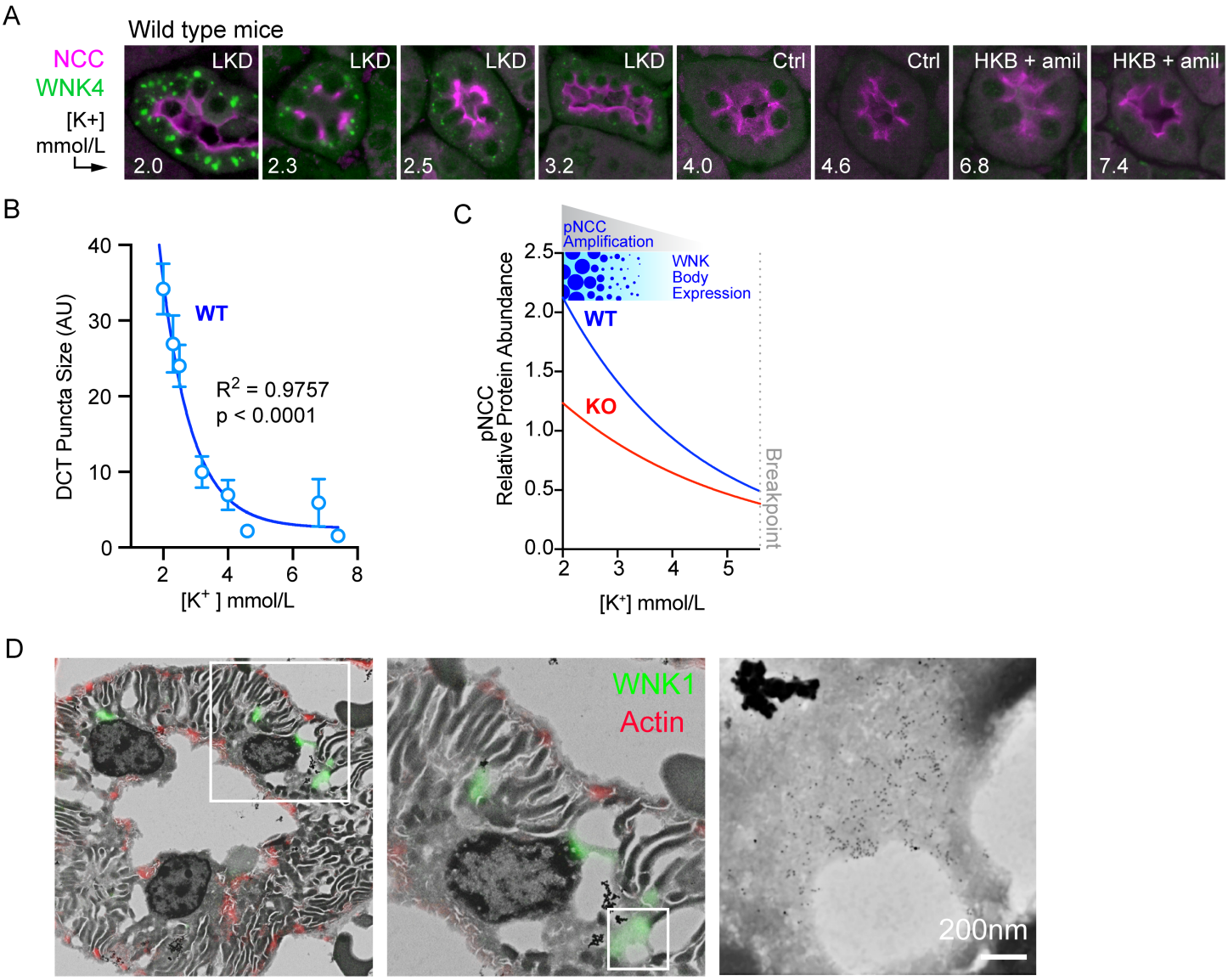


**Figure 4: WNK body condensate expression is dependent upon blood [$K^+$] and correlates with pNCC amplification during potassium deficiency**. **(A)** IF of WNK bodies in WT male mice treated with various potassium maneuvers for 10d to induce a broad range of blood $K^+$ concentrations. DCTs were identified by NCC co-staining. WNK4-positive puncta progressively increased in size as [$K^+$] fell and were not visible above a [$K^+$] of 4.0. **(B)** Quantification of WNK body size as a function of blood [$K^+$], fit to a single exponential curve; $R^2 = 0.9757$, $P < 0.0001$ vs horizontal line. This demonstrates a WNK body size dependence on [$K^+$]. **(C)** Cropped and adapted image of Figure 3B integrated with WNK body expression and pNCC amplification. As [$K^+$] falls below 4.0mmol/L, WT mice amplify NCC phosphorylation more effectively than KS-WNK1 KO mice, correlating with WNK body expression. **(D)** CLEM of a semithin (~300nm) DCT section in a hypokalemic WT mouse combining confocal with backscattered-electron scanning electron microscopy (BSE-SEM). WNK bodies were detected with a WNK1 primary and a dual Alexa-488/5nm gold particle-conjugated secondary. The image is inverted; thus, areas of low signal intensity represent lower BSE reflectivity. WNK body condensates contained immunogold signal that clustered within membraneless perinuclear cytosolic regions of lower material density.

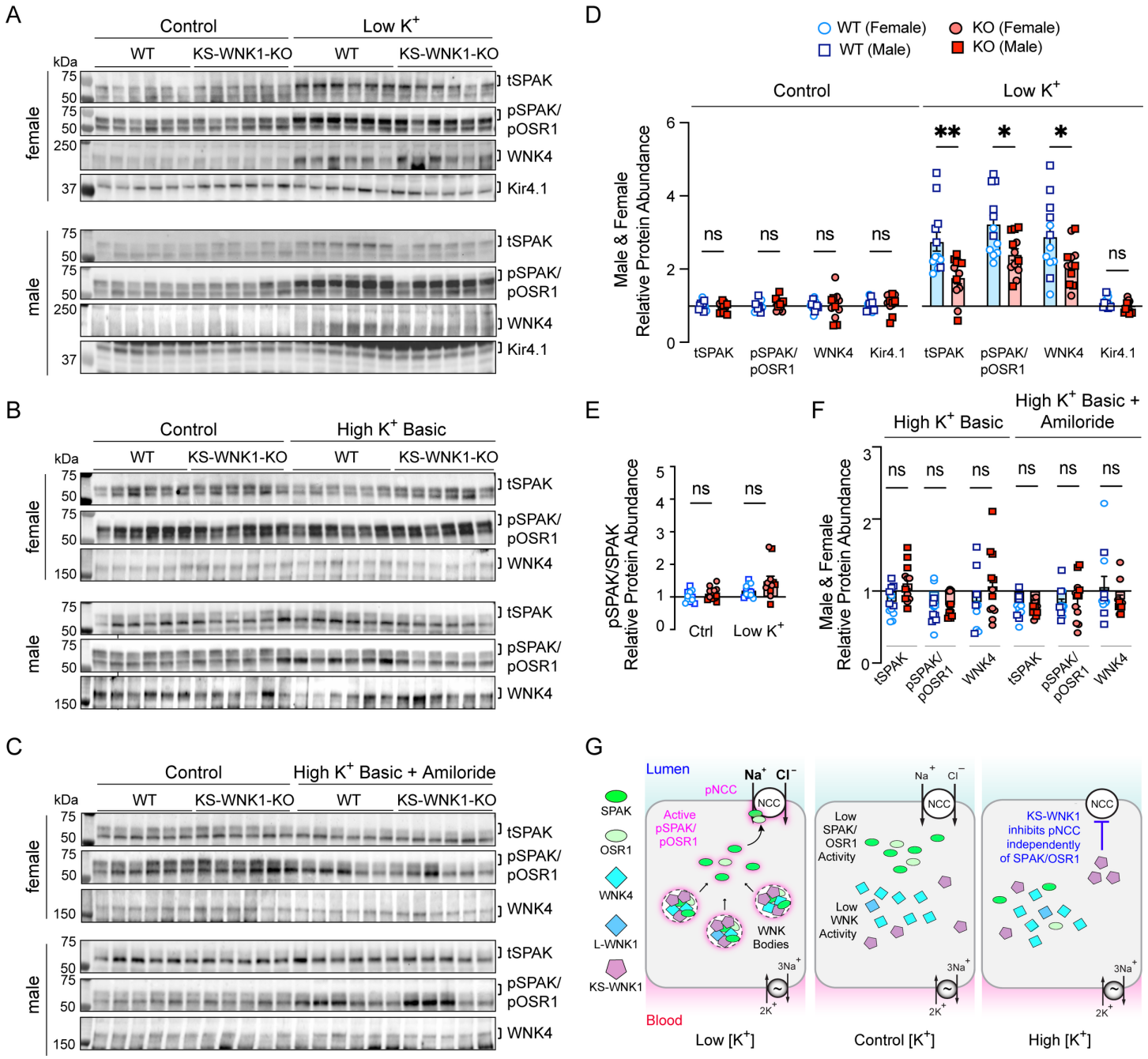


**Figure 5. Dysregulated WNK4-SPAK/OSR1 pathway activity in KS-WNK1 KO mice during K+ restriction, but not during $K^+$ loading.** IB analysis of kidney cortical extracts from female and male WT littermates and KS-WNK1 KO mice subjected to various $K^+$ maneuvers for 10d. **(A-C)** IB of the WNK-SPAK/OSR1 pathway from mice treated with either control diet versus **(A)** low $K^+$ diet, **(B)** HKB diet, or **(C)** HKB + amiloride. Brackets indicate the band analyzed. In A-C, lanes corresponding to WT and KO animals on control diet were from replicate lysates to facilitate normalization between blots. The values graphed for control diet represent an average of the replicates (see Figure S6). **(D)** WT mice fed a low $K^+$ diet had significant increases in tSPAK, pSPAK/pOSR1, and WNK4 compared to WT mice on control diet. KS-WNK1 KO mice had a blunted response to the low $K^+$ diet compared to WT mice. **(E)** phosphorylated-to-total SPAK ratio in WT and KO mice subjected to control vs low $K^+$ diet. **(F)** no differences in WNK4-SPAK/OSR1 pathway abundance or phosphorylation in WT and KS-WNK1 KO mice subjected to HKB or HKB + amiloride treatment. **(G)** WNK-SPAK/OSR1 pathway activation during low, control, and high blood [$K^+$] experimental maneuvers. During low [$K^+$], KS-WNK1-dependent WNK bodies condense the WNK-SPAK/OSR1 pathway; this correlates with SPAK/OSR1 and NCC phosphoactivation. During high $K^+$, KS-WNK1 inhibits pNCC activation independently of the SPAK/OSR1 pathway. Results are shown as means ± SE; $n$ = 12 mice per genotype and diet (males and females combined). Two-way ANOVA with Sidak's multiple comparisons test, $*P \leq 0.05$, $**P \leq 0.01$.

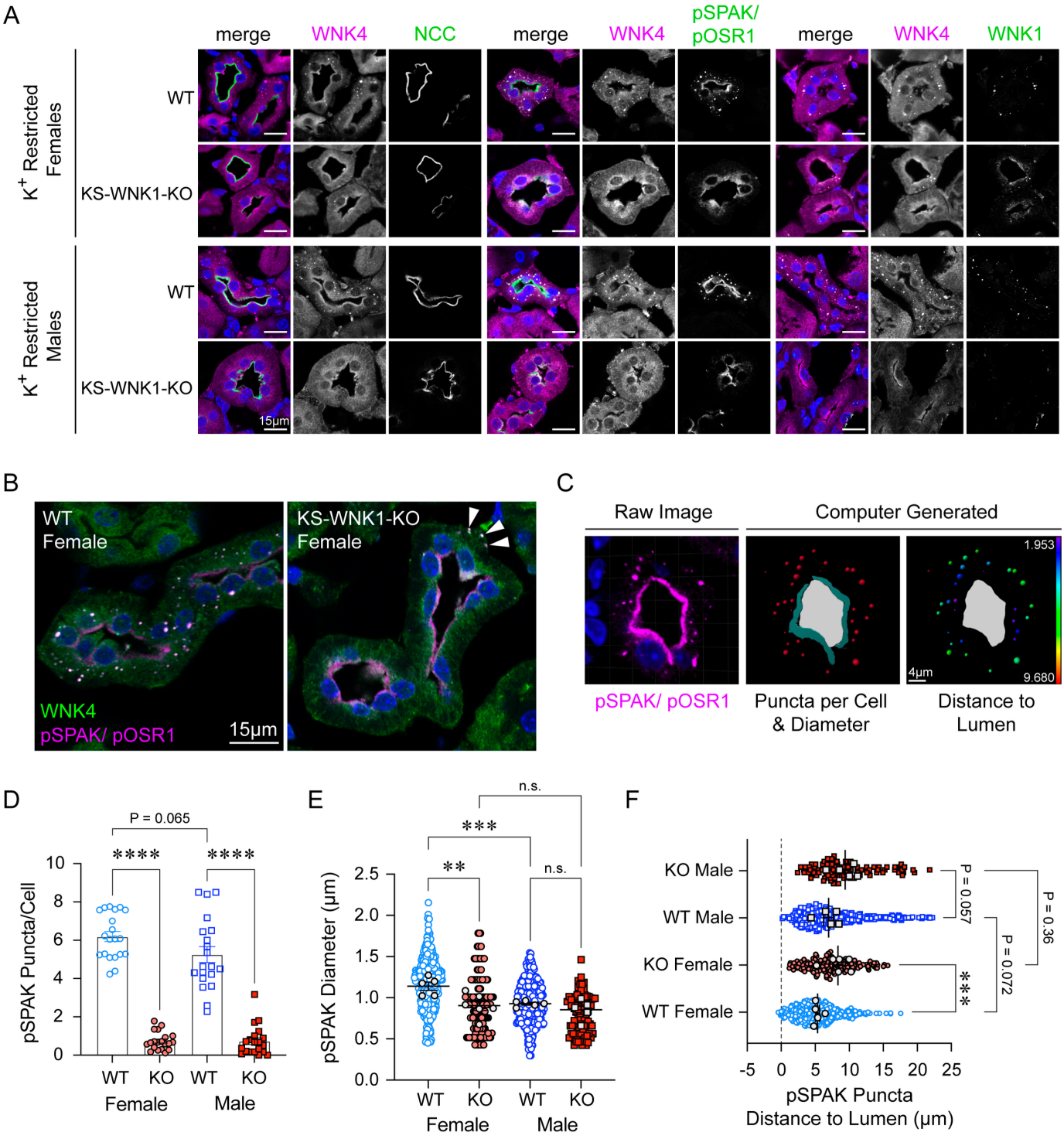


**Figure 6. $K^+$ restricted WT and KS-WNK1 KO mice exhibit sex differences in WNK body expression.**
**(A)** IF of kidney sections from WT or KS-WNK1 KO mice treated with low $K^+$ diet for 10d. DCTs were identified by NCC co-staining and morphology. WNK4, pSPAK/pOSR1, and WNK1 antibodies colocalized within puncta in WT mice, whereas puncta were nearly absent in KS-WNK1 KO mice (duplicate bottom left image with Figure 1C). All bars = 15μm. **(B)** WNK body formation in female WT and KS-WNK1 KO mice. Cytosolic puncta are largely absent in KS-WNK1 KO mice, though pSPAK/pOSR1 apical staining is present. Uncommonly, mislocalized basolateral puncta containing pSPAK/pOSR1 and WNK4 were observed (arrowheads). Bar = 15μm. **(C)** Imaris was used to quantify WNK body number and size (*middle*) and distance to lumen (*right*), from raw confocal IF images of pSPAK/pOSR1 puncta (*left*). Bar = 4μm. **(D-F)** Quantification of pSPAK/pOSR1. **(D)** Puncta per cell (20 tubules per condition), **(E)** Puncta diameter (5 tubules per condition), and **(F)** Distance to apical lumen in female and male mice (5 tubules per condition). Two-way ANOVA with Sidak's multiple comparison, $*P \leq 0.05$, $**P \leq 0.01$, $***P \leq 0.001$, $****P \leq 0.0001$.

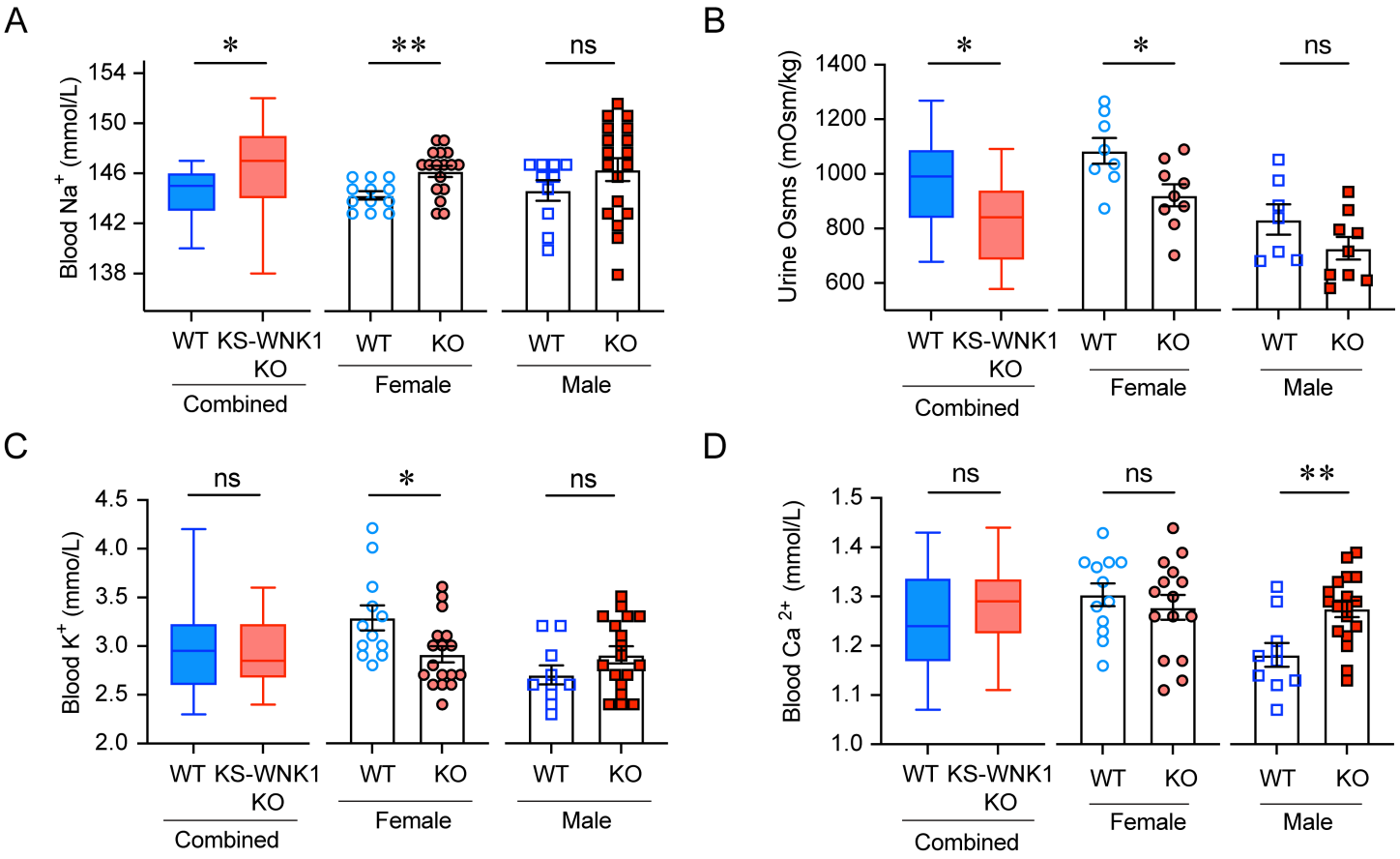


**Figure 7. Effect KS-WNK1 on blood and urine composition in $K^+$ restricted female and male mice.** Male and female Whole blood electrolytes and urine were obtained from WT and KS-WNK1 KO mice fed low $K^+$ diets for 10d. Results were analyzed as both combined and sex-disaggregated. **(A)** KS-WNK1 KO mice had significantly increased blood [$Na^+$] when males and females were analyzed in combination, and when females were analyzed separately. **(B)** Urine osmolality in KS-WNK1 KO mice was significantly decreased in the combined male and female dataset, and in the female pool. Mean $U_{osm}$ in KS-WNK1 KO males was lower than male WT without reaching significance. **(C)** KS-WNK1 deletion had no significant effect on whole blood [$K^+$] in the combined pool, or in the male pool. However, female KS-WNK1 KO mice had a significant decrease in whole blood [$K^+$] compared to sex-matched controls. **(D)** KS-WNK1 deletion had no significant effect on whole blood [$Ca^{2+}$] in the combined male and female pool or in the female pool. However, male KS-WNK1 KO mice had a significant increase in whole blood [$Ca^{2+}$]. Sample size: $n$ = 10-18 mice. Unpaired t-test between WT and KO was used to determine significance, *$P \leq 0.05$, **$P \leq 0.01$.

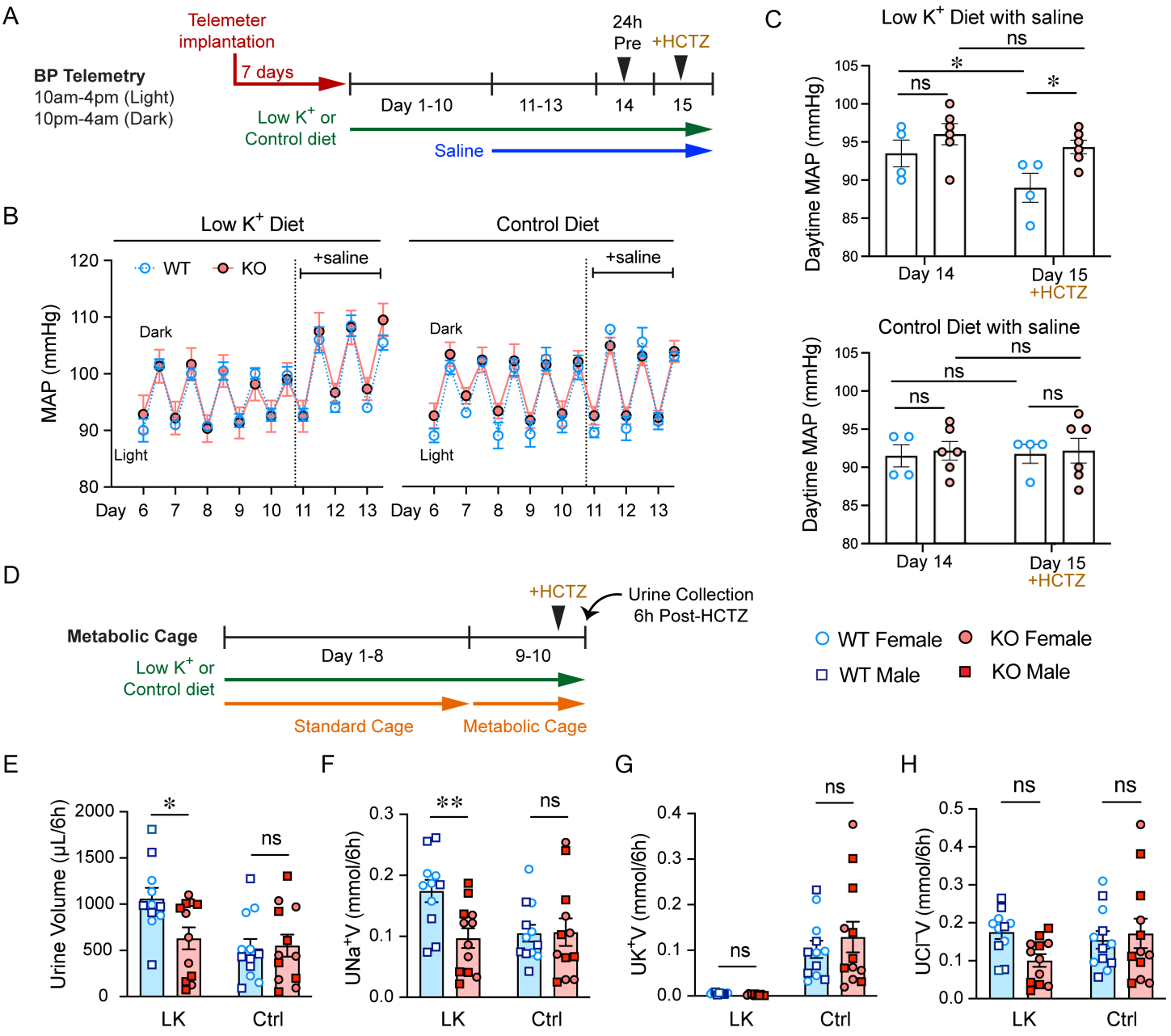


**Figure 8. Potassium restricted KS-WNK1 knockout mice are thiazide-insensitive. (A)** Schematic of the BP telemetry experiment. Female WT ($n$ = 4) and KS-WNK1 KO mice ($n$ = 6) were subjected to either low $K^+$ or control diets for 10d, followed by supplementation with 1% normal saline (NS) in drinking water for 3d, then hydrochlorothiazide (HCTZ) treatment. **(B)** KS-WNK1 expression had no significant effect on mean arterial pressure (MAP) in $K^+$ restricted or control fed mice. Saline supplementation increased MAP in $K^+$ restricted mice. Genotype had no significant effect determined by two-way ANOVA with post-hoc Sidak's. Each data point represents either daytime or nighttime MAP averaged over 6h. **(C)** Thiazide challenge. Mice were fed low $K^+$ or control diet for 10d and then 1% saline in their drinking water for 3d. Daytime MAP was measured for a 6h window starting on day 14 (24h before) HCTZ injection, and on day 15 (1h after) HCTZ (25 mg/kg IP). WT mice on low $K^+$ diet had a significant decrease in MAP with HCTZ, compared to KS-WNK1 KO. *$P \leq 0.05$, two-way ANOVA with post-hoc Sidak's. **(D)** Schematic of the metabolic cage experiment. Diuretic challenge was performed in both female and male WT and KS-WNK1 KO mice. After 10d of control or low $K^+$ diet, mice were injected with HCTZ (25 mg/kg IP), and urine was collected for 6h. **(E-H) (E)** urine volume and **(F)** urine Na*V (UNaV) were greater in WT mice compared to KO mice. **(G)** On the low $K^+$ diet, urine $K^+$ was too low to detect a significant difference. **(H)** There was a trend for HCTZ to blunt $Cl^-$ excretion in KS-WNK1 KO mice on low $K^+$ diet, without reaching significance. Results are shown as means ± SE; $n$ = 12 mice per genotype and diet. Two-way ANOVA with Sidak's post-test; *$P \leq 0.05$, **$P \leq 0.01$. See also Tables S2-S3.

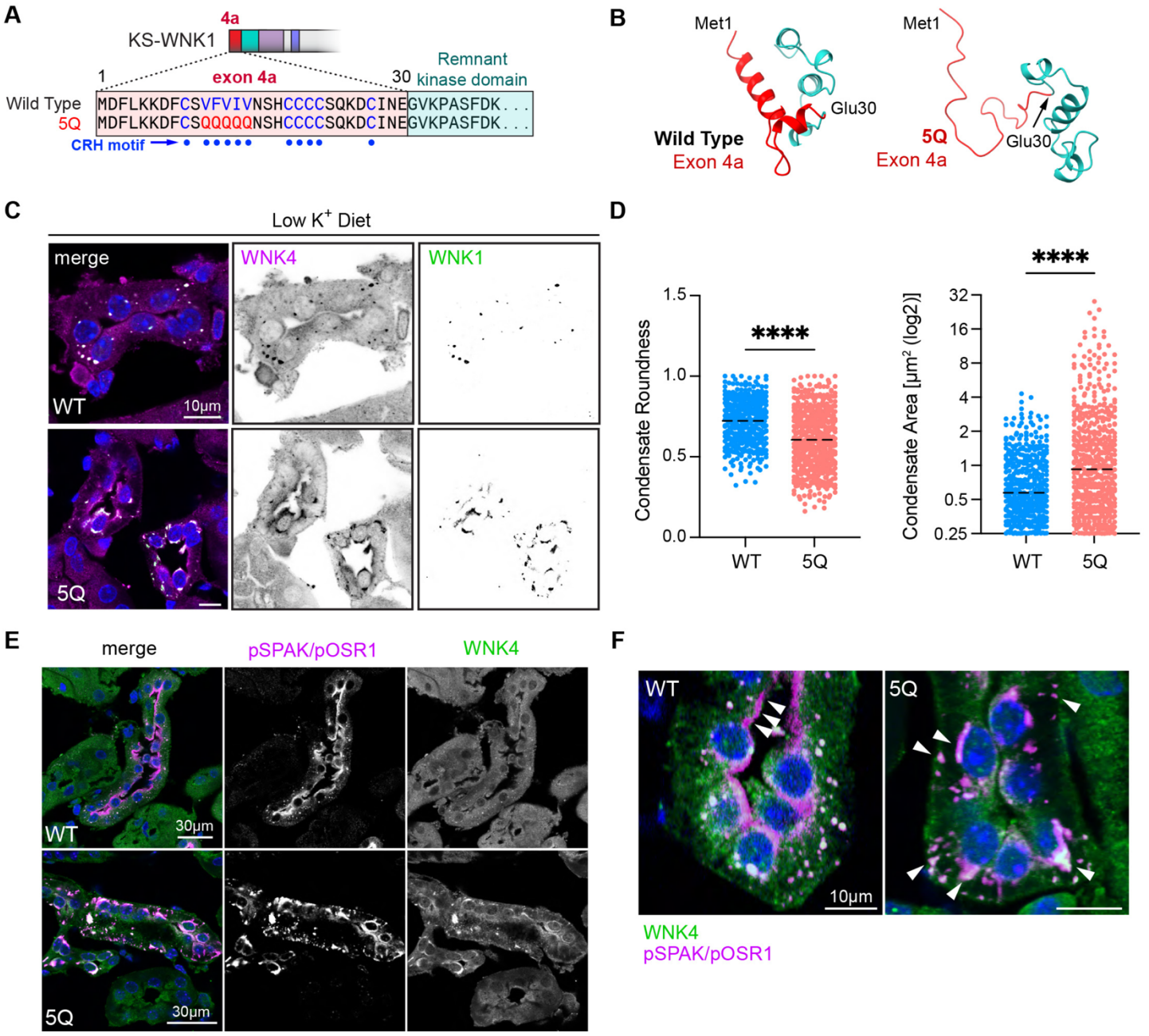


**Figure 9. KS-WNK1 5Q mutant mice exhibit altered WNK body morphology and pSPAK localization.**
**(A)** Exon 4a of KS-WNK1 encodes a 30AA, including a cysteine-rich hydrophobic (CRH) motif. The motif's five consecutive bulky hydrophobic residues was mutated to glutamines to generate "5Q" mice with aberrant WNK body formation. **(B)** AlphaFold predicted structures of the WT and 5Q exon 4a peptide (red) and the adjacent remnant kinase domain (cyan). The 5Q mutation disrupts a predicted helical structure encoded by exon 4a. **(C)** IF of kidneys from female 5Q mice maintained on low $K^+$ diet for 10d. Typical WNK bodies are absent and replaced by irregularly shaped foci that often form paranuclear crescents and contain WNK4 and pSPAK/pOSR1. **(D)** The morphology of the 5Q foci were less round and larger than wild-type WNK bodies. $n$ =425 foci from 9 images for WT, 530 from 12 images for 5Q, ****$P < 0.0001$. **(E)** WNK4 and pSPAK/pOSR1 costaining in WT and 5Q mice. In WT, pSPAK/pOSR1 signal colocalized with WNK4 in puncta and was also located at the DCT apical membrane. In contrast 5Q mice exhibited strong pSPAK/pOSR1 and WNK4 co-condensation in perinuclear aggregates, but no apical pSPAK/pOSR1. **(F)** Higher magnification image of WNK4 and activated SPAK/OSR1 expression. White arrows highlight that in WT mice, pSPAK/pOSR1 accumulates at the plasma membrane, but in 5Q mice, it becomes sequestered in irregularly shaped, generally subnuclear foci.

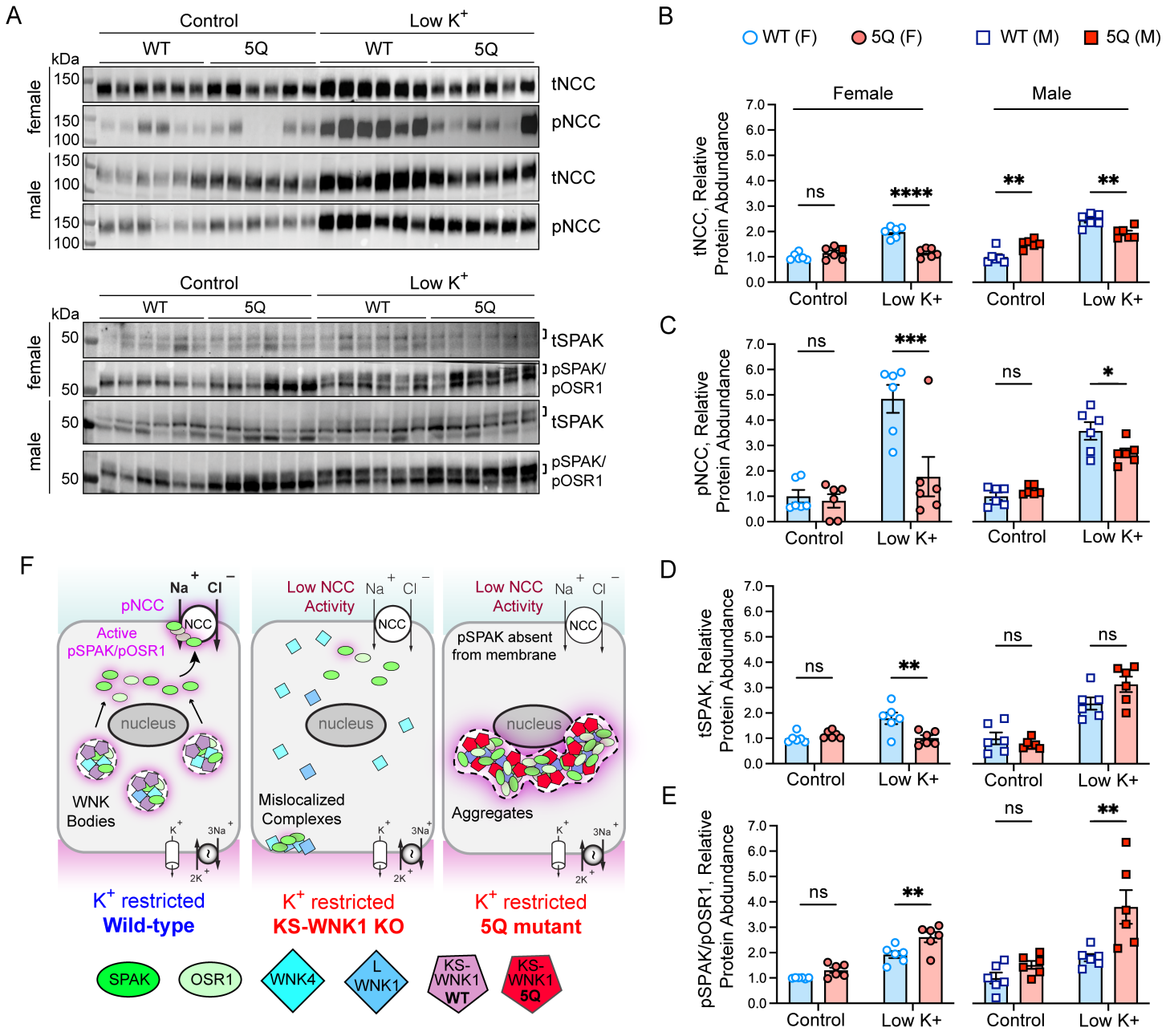


**Figure 10. WNK bodies are necessary for KS-WNK1 to amplify NCC phosphorylation during hypokalemia.**
**(A)** WT and 5Q mice were fed control or low $K^+$ diet for 10d and kidney cortex homogenates were probed for tNCC, pNCC, tSPAK, and pSPAK/pOSR1. Brackets indicate the band analyzed **(B-E)** Graphical representation of immunoblots in **(A)**. **(B)** tNCC abundance. **(C)** pNCC abundance. **(D)** tSPAK abundance. (E) pSPAK/pOSR1 abundance. $K^+$ restricted 5Q mice had significantly increased pSPAK/pOSR1 and reduced tNCC and pNCC expression, indicating that signaling to NCC was uncoupled. $n = 6$ mice per genotype, sex, and diet. Two-way ANOVA with Sidak's post-test was applied, $*P < 0.05$, $**P < 0.01$, $***P \leq 0.001$, $****P \leq 0.0001$. **(F)** Model of WNK-SPAK/OSR1-NCC signaling in WT, KS-WNK1 KO, and 5Q mice. KS-WNK1 normally facilitates WNK body condensate formation and NCC activation via the WNK-SPAK/OSR1 pathway. In $K^+$ restricted KS-WNK1 KO mice, WNK bodies are largely absent and remaining complexes are mislocalized, resulting in low SPAK/OSR1 and NCC activity. In the $K^+$ restricted 5Q mouse, WNK-pSPAK/pOSR1 becomes trapped in perinuclear aggregates preventing pSPAK/pOSR1 expression at the DCT apical membrane, causing a reduction in NCC activity. See also Table S4.

A

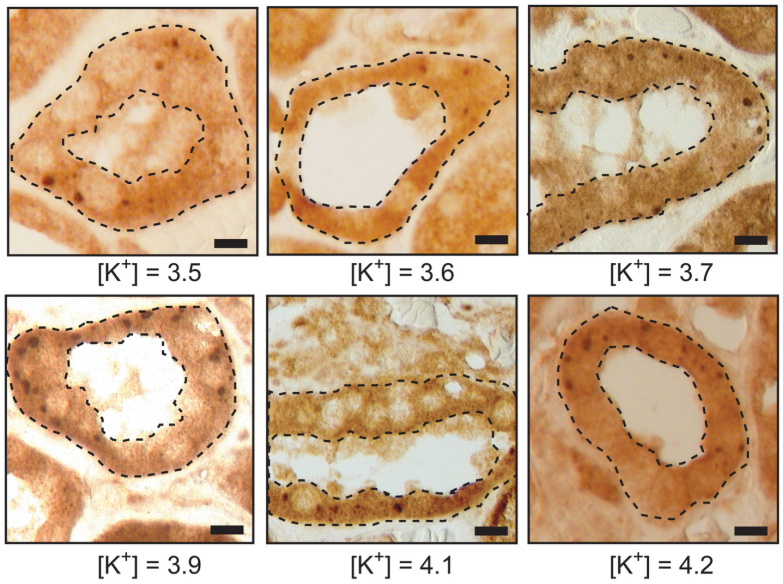


B

Human WNK body quantification

| Serum [K+] (mmol/L) | Sex | Age | # Tubules Analyzed | Total # of WNK bodies | Total # nuclei | WNK bodies/ nuclei |
|---|---|---|---|---|---|---|
| 3.5 | F | 57 | 4 | 103 | 76 | 1.36 |
| 3.6 | M | 63 | 4 | 52 | 45 | 1.16 |
| 3.7 | F | 79 | 4 | 127 | 72 | 1.76 |
| 3.9 | M | 68 | 3 | 61 | 56 | 1.09 |
| 4.1 | M | 46 | 3 | 16 | 46 | 0.35 |
| 4.2 | M | 55 | 4 | 32 | 59 | 0.67 |

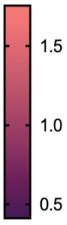


C

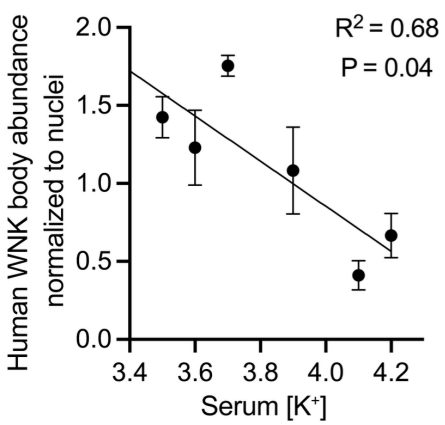


**Figure 11. Human WNK body abundance correlates with serum [$K^+$].**
**(A)** Immunohistochemistry of DCTs obtained from 6 human kidney wedge biopsies stained for WNK1. DCTs were confirmed by NCC staining in adjacent sections (not shown). **(B)** Serum [$K^+$], sex, and age of the subjects, along with the values used for quantification. A heat map indicates the correlation between WNK bodies with increasing serum [$K^+$]. **(C)** There was an inverse relationship between serum [$K^+$] and WNK body abundance. To calculate the average number of WNK bodies per cell, the number of WNK bodies within a single tubule were counted and then normalized to the number of nuclei within that tubule. Each data point represents the average number of WNK bodies per kidney analyzed; $n$ = 3-4 tubules analyzed per kidney. Slope of -1.446 calculated using simple linear regression. Results are shown as means ±SE; $R^2 = 0.68$, $P = 0.04$ vs horizontal line.